Table 1. Serum lipid levels in apoE$^{-/-}$ mice treated with vehicle or 4 mg/kg/day loxoprofen sodium from 8 to 16 weeks of age

	Male			Female		
	Vehicle	Loxoprofen Na 56 days	p	Vehicle	Loxoprofen Na 56 days	p
N	11	11		11	11	
Body weight [g]	27.3 ± 0.48	27.17 ± 0.34	0.73	21.80 ± 0.91	20.04 ± 0.57	0.12
Albumin [mg/dL]	3.01 ± 0.03	2.94 ± 0.03	0.07	3.12 ± 0.03	3.12 ± 0.04	0.98
Creatinine [mg/dL]	0.07 ± 0.01	0.09 ± 0.01	0.15	0.08 ± 0.01	0.08 ± 0.01	0.98
Free fatty acids [μEQ/L]	662.64 ± 110.4	553.17 ± 117.59	0.51	413.02 ± 58.2	383.19 ± 107.33	0.81
Total cholesterol [mg/dL]	1253.26 ± 51.51	1162.89 ± 52.74	0.23	1045.65 ± 39.81	1091.43 ± 103.33	0.69
Triglycerides [mg/dL]	39.60 ± 6.44	34.95 ± 3.39	0.53	21.11 ± 1.93	21.26 ± 2.15	0.96

From the 8th week to 16th week, mice were randomized to receive a western diet and vehicle or 4 mg/kg/day of loxoprofen sodium (n = 11 animals for each group). Mice were fasted for 4 h, and lipoprotein distribution was determined by HPLC. Serum albumin, creatinine, and free fatty acids were analyzed with dry chem system. Results are expressed as mean ± SEM. Student t test was used for comparisons between two groups.

Results

Loxoprofen sodium inhibits platelet thromboxane production in apoE$^{-/-}$ mice and healthy humans

To test the effect and the COX-2 selectivity of loxoprofen sodium, we measured platelet Tx, PGI_2, and PGE_2 production in apoE$^{-/-}$ mice and healthy men. Loxoprofen sodium inhibited the platelet production of TxA_2 metabolite, urinary TxB_2, by 29.0% compared to vehicle in apoE$^{-/-}$ mice (269.55 ± 77.48 ng/mg CRE vs 929.17 ± 196.29 ng/mg CRE, p = 0.012), and inhibited the production of urinary TxB_2 by 26.2% compared to pre medication in men (0.53 ± 0.10 ng/mg CRE vs 2.04 ± 0.12 ng/mg CRE, p = 0.001) (Fig. 1A and D). Loxoprofen sodium inhibited the production of PGE_2 metabolite in apoE$^{-/-}$ mice by 9.0% compared to vehicle (1.29 ± 0.29 ng/mg CRE vs 14.49 ± 3.60 ng/mg CRE, p = 0.003, respectively), and inhibited the production of urinary PGE_2 metabolite by 29.7% compared to pre medication in men (0.06 ± 0.02 ng/mg CRE vs 0.20 ± 0.03 ng/mg CRE, p = 0.028) (Fig. 1C and F). Loxoprofen sodium also inhibited the production of PGI_2 metabolite, urinary 2,3 dinor 6 keto $PGF_{1\alpha}$, in apoE$^{-/-}$ mice by 26.9% compared to vehicle (107.0 ± 17.83 ng/mg CRE vs 397.2 ± 122.1 ng/mg CRE, p<0.001), and inhibited the production of urinary 2,3 dinor 6 keto $PGF_{1\alpha}$ by 44.0% compared to pre medication in men (1.11 ± 0.04 ng/mg CRE vs 2.52 ± 0.09 ng/mg CRE, p<0.001) (Fig. 1B and E).

Loxoprofen sodium inhibits platelet aggregation in apoE$^{-/-}$ mice and healthy humans

Fig. 2 A, B, C and D shows representative results of mouse platelet aggregation stimulated by ADP or collagen solutions. Although $PATI_{ADP}$ was 1.96 ± 0.66 μM and $PATI_{collagen}$ was 2.17 ± 0.44 μg/ml in mice with vehicle, they were suppressed to >4 μM (n = 15, p = 0.033), and >4 μg/ml (n = 15, p<0.001) after administration of loxoprofen sodium. Fig. 2 E, F, G and H show representative results of healthy human platelet aggregation stimulated by ADP or collagen solutions, respectively. After administration of loxoprofen sodium, platelet aggregation was suppressed. Although $PATI_{ADP}$ was 1.52 ± 0.39 μM and $PATI_{collagen}$ was 0.41 ± 0.03 μg/ml in humans before administration of loxoprofen sodium, they were suppressed to 3.18 ± 1.50 μM (n = 5, p = 0.004), and 1.28 ± 0.50 μg/ml (n = 5, p = 0.034) after its administration.

Loxoprofen sodium does not affect serum levels of total cholesterol, triglycerides, or free fatty acids in apoE$^{-/-}$ mice

Body weights were unchanged in mice treated with both loxoprofen sodium and vehicle (Table 1). Dry chem system demonstrated that the serum levels of albumin, CRE, and FFA were unchanged in mice treated with loxoprofen sodium and vehicle. HPLC analysis demonstrated that the serum levels of total cholesterol and serum triglycerides were unchanged (Table 1).

Loxoprofen sodium reduces extent of atherosclerosis in apoE$^{-/-}$ mice

Atherosclerotic lesion area of the aortic root was significantly decreased to 41.5% (308,545 ± 36,892 μm^2, p<0.001) in female mice receiving 4 mg/kg/day of loxoprofen sodium for 56 days and was decreased to 75.6% (487,455 ± 29,623 μm^2, p = 0.001) in female mice receiving 4 mg/kg/day of loxoprofen sodium for 7 days compared to mice treated with vehicle (644,372 ± 28,314 μm^2) (Fig. 3D). Similarly, atherosclerotic lesion area was significantly decreased to 63.5% (372,145 ± 38,149 μm^2, p = 0.015) in male mice receiving loxoprofen sodium for 56 days and 84.8% (432,789 ± 39,236 μm^2, p = 0.015) in male mice receiving it for 7 days compared to mice treated with vehicle (vs 510,117 ± 34,409 μm^2) (Fig. 3E).

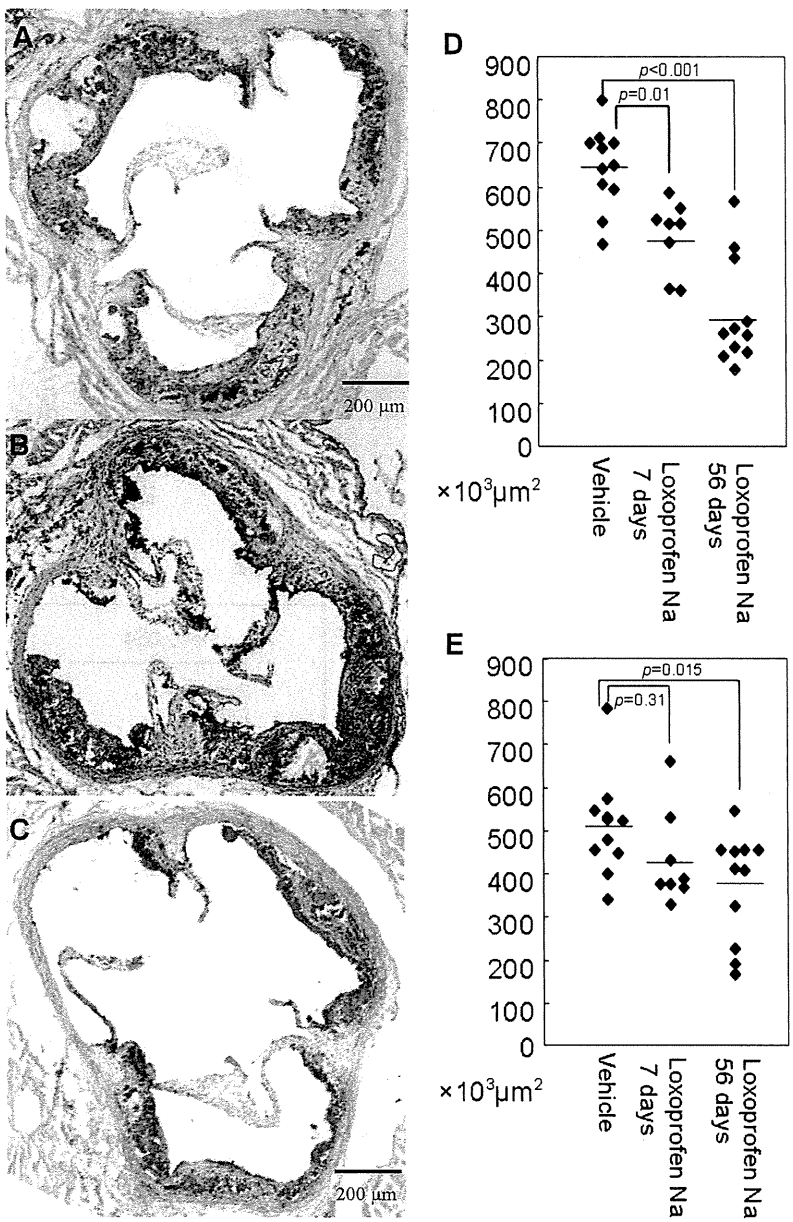

Fig. 3. Representative Oil-Red-O stained sections from the proximal aorta of female apoE$^{-/-}$ mice, and quantification of atherosclerotic lesion area. A, B, and C were representative Oil-Red-O stained sections from the proximal aorta of female apoE$^{-/-}$ mice. (A), female mice treated with vehicle, (B) female mice with 4 mg/kg/day loxoprofen sodium for 7 days, and (C) female mice with it for 56 days. Scale bar = 200 μm. E indicated the area of atherosclerotic lesions in male mice receiving vehicle (510,117 ± 34,409 μm^2), loxoprofen sodium (4 mg/kg/day) for 7 days (432,789 ± 39,236 μm^2), loxoprofen sodium for 56 days (372,145 ± 38,149 μm^2). Similarly, D indicated those in female mice, with the mean and SEM being 644,372 ± 28,314 μm^2, 487,455 ± 29,623 μm^2, and 308,545 ± 36,892 μm^2, respectively. Individual data were expressed as dots in each group, and the average was expressed as mean ± SEM. Dunnett test was used to for comparisons with mice receiving vehicle. Horizontal bar indicated the mean in each group.

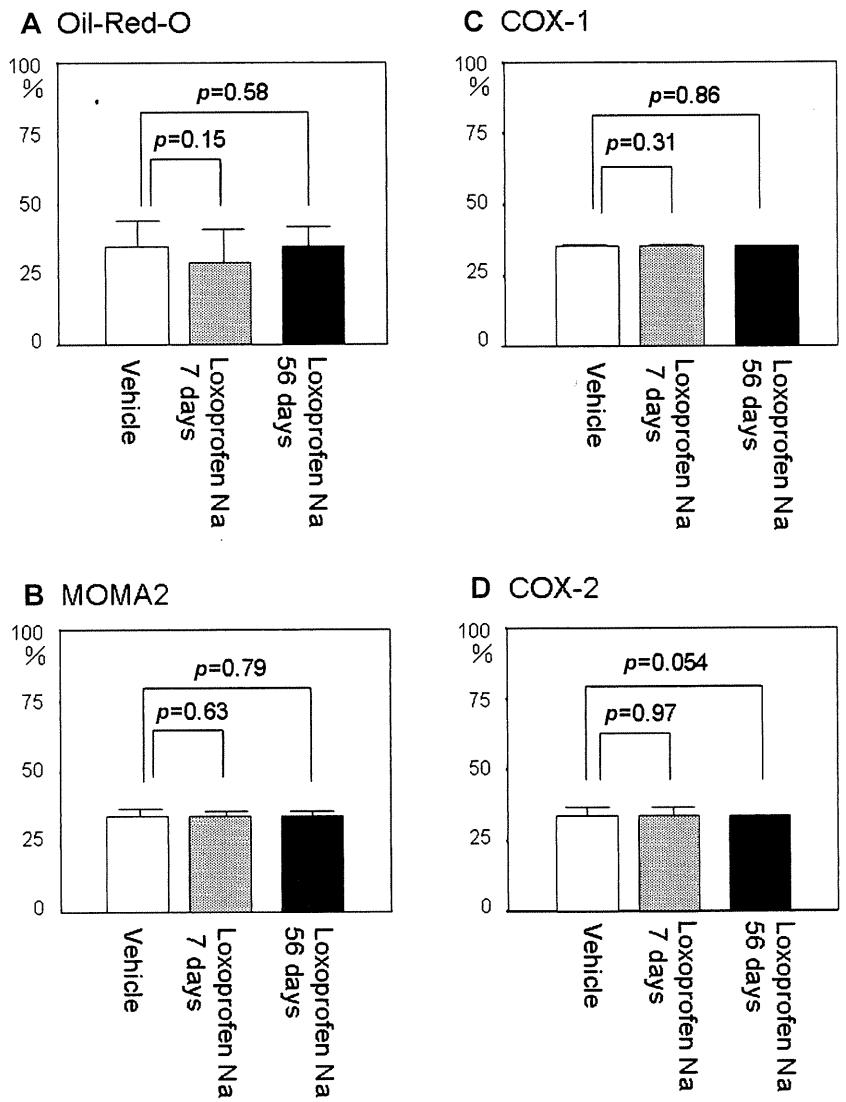

Fig. 4. The extent of Oil-Red-O stained lesions, and MOMA2, COX-1 and COX-2 positive lesions in atherosclerotic lesions of female apoE$^{-/-}$ mice. We applied Oil-Red-O stain and immunocytochemical detection of macrophages or COX in female apoE$^{-/-}$ mice treated with vehicle (open bars), with 4 mg/kg/day loxoprofen sodium for 7 days (gray bars), and for 56 days (solid bars). We compared the prevalence of Oil-Red-O stained lesions (A). Sections from proximal aorta were stained with monoclonal antibodies to macrophages (MOMA-2) (B), COX-1 (C) or COX-2 (D). Data were expressed as the average (mean ± SEM). Dunnett test was used for comparisons among the three groups.

Representative Oil-Red-O and hematoxylin stained sections from the proximal aorta of female mice treated with vehicle (Fig. 3A), female mice receiving 4 mg/kg/day loxoprofen sodium for 7 days (Fig. 3B), and female mice receiving 4 mg/kg/day loxoprofen sodium for 56 days (Fig. 3C), indicate fatty streak lesions consisting predominantly of foam cells. The prevalence of Oil-Red-O stained lesions among arteriosclerotic lesions in male and female mice with loxoprofen sodium was equal to that in male and female mice receiving vehicle (Fig. 4A).

Inmunohistochemical analysis of MOMA2, COX-1 and COX-2 in atherosclerotic lesions of apoE$^{-/-}$ mice

The prevalence of positive staining lesions of MOMA2, COX-1 and COX-2 in atherosclerotic lesions in female mice treated with loxoprofen sodium for both 7 days and 56 days was similar to that in female mice treated with vehicle (Fig. 4B, C and D).

Side effects of loxoprofen sodium in apoE$^{-/-}$ mice

Treatment of apoE$^{-/-}$ mice with 4 mg/kg/day loxoprofen sodium was well tolerated. The histological examination of liver, kidney and stomach showed no abnormalities even at a dose of 8 mg/kg of loxoprofen sodium.

Discussion

Atherosclerotic lesion formation was reduced to 63.5% and 41.5%, in male and female apoE$^{-/-}$ mice with loxoprofen sodium compared to control, respectively. However, the composition of atherosclerotic lesions in mice treated with loxoprofen sodium differed from that in the mice receiving vehicle. The extent of Oil-Red-O, COX-1 and COX-2 expression was the same in mice receiving loxoprofen sodium and vehicle. Loxoprofen sodium reduced the production of TxB_2 and PGI_2, and also reduced platelet aggregation *in vivo*. Loxoprofen sodium has anti-inflammatory effects and reduced the production of PGE_2. Thus, loxoprofen sodium, a non-selective NSAID, may reduce atherosclerotic lesion formation in apoE$^{-/-}$ mice by an anti-inflammatory effect. It is widely accepted that aspirin prevent the occurrence of myocardial infarction and/or ischemic stroke primarily through the inhibition of platelet aggregation, although their role in the development of fatty streak lesions remains a matter of debate.

Belton *et al.* demonstrated that the profile of PG generation and expression of COX were remarkably similar in the apoE$^{-/-}$ murine model and human atherosclerosis. In the apoE$^{-/-}$ murine model and human atherosclerosis, there is an increase in the biosynthesis of TXA_2 and PGI_2, with induction of COX-1 and COX-2 [*18*]. The COX-2 selectivity of loxoprofen sodium active metabolite (loxoprofen-SRS) *in vitro* (the ratio of COX-1 IC50 /COX-2 IC50) was 0.35 [*19*]. Our study indicated that administration of loxoprofen sodium for apoE$^{-/-}$ mice (4 mg/kg/day) reduced biosynthesis of PEG_2 metabolite to 9.0%, TXA_2 metabolite to 29.0%, and PGI_2 metabolite to 26.9%. Moreover, administration of loxoprofen sodium to healthy men (60 mg/body, three times a day) reduced the biosynthesis of PGE_2 metabolite to 29.7%, TXA_2 metabolite to 26.2%, and PGI_2 metabolite to 44.0%. Thus, loxoprofen sodium may be a well-balanced COX-1 and COX-2 inhibitor, which contributes to a reduction of atherosclerotic lesion formation.

On the other hand, loxoprofen sodium did not change the serum levels of total cholesterol or serum triglycerides. Some COX inhibitors might affect lipid metabolism. Rofecoxib has been reported to increase the susceptibility of human LDL-c and cell membrane lipids to oxidative modification, a hallmark feature of atherosclerosis. Rofecoxib promoted the non-enzymatic formation of isoprostanes from biological lipids, which act as important mediators of inflammation in the atherosclerotic plaque [*20*]. Celecoxib does not have these effects. Thus, each NSAID has different pharmacologic actions [*20–22*].

In conclusion, loxoprofen sodium, a non-selective NSAID, reduces atherosclerotic lesion formation in apoE$^{-/-}$ mice by suppression of PGE_2, TxB_2 and PGI_2. The influence of COX-2 selective inhibition in atherosclerosis has been controversial, but non-selective NSAID could reduce atherosclerotic lesion formation in a murine model. Our data may provide insights into the mechanisms underlying the cardiovascular safety of NSAIDs.

Abbreviations

RA, rheumatoid arthritism; SLE, systemic lupus erythematosus; COX-2, cyclooxygenase-2; NSAIDs, nonsteroidal anti-inflammatory drugs; Tx, thromboxane; PG, prostaglandin; PRP, platelet rich plasma; ADP, adenosine diphosphate; PATI, platelet aggregatory threshold index; HPLC, high performance liquid chromatograph.

References

[1] del Rincon, I.D., Williams, K., Stern, M.P., Freeman, G.L., and Escalante, A.: High incidence of cardiovascular events in a rheumatoid arthritis cohort not explained by traditional cardiac risk factors. *Arthritis Rheum.*, **44**, 2737–2745, 2001.

[2] Van Doornum, S., McColl, G., and Wicks, I.P.: Accelerated atherosclerosis: an extraarticular feature of rheumatoid arthritis? *Arthritis Rheum.*, **46**, 862–873, 2002.

[3] Gabriel, S.E., Crowson, C.S., Kremers, H.M., Doran, M.F., Turesson, C., O'Fallon, W.M., and Matteson, E.L.: Survival in rheumatoid arthritis: a population-based analysis of trends over 40 years. *Arthritis Rheum.*, **48**, 54–58, 2003.

[4] Stanic, A.K., Stein, C.M., Morgan, A.C., Fazio, S., Linton, M.F., Wakeland, E.K., Olsen, N.J., and Major, A.S.: Immune dysregulation accelerates atherosclerosis and modulates plaque composition in systemic lupus erythematosus. *Proc. Natl. Acad. Sci. U.S.A.*, **103**, 7018–7023, 2006.

[5] Westerweel, P.E., Luyten, R.K., Koomans, H.A., Derksen, R.H., and Verhaar, M.C.: Premature atherosclerotic cardiovascular disease in systemic lupus erythematosus. *Arthritis Rheum.*, **56**, 1384–1396, 2007.

[6] Nussmeier, N.A., Whelton, A.A., Brown, M.T., Langford, R.M., Hoeft, A., Parlow, J.L., Boyce, S.W., and Verburg, K.M.: Complications of the COX-2 inhibitors parecoxib and valdecoxib after cardiac surgery. *N. Engl. J. Med.*, **352**, 1081–1091, 2005.

[7] Mukherjee, D., Nissen, S.E., and Topol, E.J.: Risk of cardiovascular events associated with selective COX-2 inhibitors. *J.A.M.A.*, **286**, 954–959, 2001.

[8] Hennekens, C.H., Dyken, M.L., and Fuster, V.: Aspirin as a therapeutic agent in cardiovascular disease: a statement for healthcare professionals from the American Heart Association. *Circulation*, **96**, 2751–2753, 1997.

[9] Arakawa, T., Fujiwara, Y., Sollano, J.D., Zhu, Q., Kachintorn,

U., Rani, A.A., Hahm, K.B., Takahashi, S., Joh, T., Kinoshita, Y., Matsumoto, T., Naito, Y., Takeuchi, K., Yamagami, H., Agustanti, N., Xiong, H., Chen, X., Jang, E.J., Furuta, K., Terano, A., and IGICS study group: A questionnaire-based survey on the prescription of non-steroidal anti-inflammatory drugs by physicians in East Asian countries in 2007. *Digestion*, **79**, 177–185, 2009.

[10] Belton, O.A., Duffy, A., Toomey, S., and Fitzgerald, D.J.: Cyclooxygenase isoforms and platelet vessel wall interactions in the apolipoprotein E knockout mouse model of atherosclerosis. *Circulation*, **108**, 3017–3023, 2003.

[11] Burleigh, M.E., Babaev, V.R., Oates, J.A., Harris, R.C., Gautam, S., Riendeau, D., Marnett, L.J., Morrow, J.D., Fazio, S., and Linton, M.F.: Cyclooxygenase-2 promotes early atherosclerotic lesion formation in LDL receptor-deficient mice. *Circulation*, **105**, 1816–1823, 2002.

[12] Chenevard, R., Hurlimann, D., Bechir, M., Enseleit, F., Spieker, L., Hermann, M., Riesen, W., Gay, S., Gay, R.E., Neidhart, M., Michel, B., Luscher, T.F., Noll, G., and Ruschitzka, F.: Selective COX-2 inhibition improves endothelial function in coronary artery disease. *Circulation*, **107**, 405–409, 2003.

[13] Tanaka, K., Terada, A., Iizuka, Y., Hayashi, R., Masuda, H., and Mizuno, K.: Loxoprofen Sodium (CS-600), A New Non-steroidal Anti-inflammatory Drug. *Sankyo Kenkyusho Nempo*, **36**, 1–43, 1984.

[14] Sudo, T., Ito, H., and Kimura, Y.: Characterization of platelet aggregation in whole blood of laboratory animals by a screen filtration pressure method. *Platelets*, **14**, 239–246, 2003.

[15] Okazaki, M., Usui, S., Ishigami, M., Sakai, N., Nakamura, T., Matsuzawa, Y., and Yamashita, S.: Identification of unique lipoprotein subclasses for visceral obesity by component analysis of cholesterol profile in high-performance liquid chromatography. *Arterioscler. Thromb. Vasc. Biol.*, **25**, 578–584, 2005.

[16] Campos, H., Dreon, D.M., and Krauss, R.M.: Associations of hepatic and lipoprotein lipase activities with changes in dietary composition and low density lipoprotein subclasses. *J. Lipid. Res.*, **36**, 462–472, 1995.

[17] Paigen, B., Morrow, A., Holmes, P.A., Mitchell, D., and Williams, R.A.: Quantitative assessment of atherosclerotic lesions in mice. *Atherosclerosis*, **68**, 231–240, 1987.

[18] Belton, O., Byrne, D., Kearney, D., Leahy, A., and Fitzgerald, D.J.: Cyclooxygenase-1 and -2-dependent prostacyclin formation in patients with atherosclerosis. *Circulation*, **102**, 840–845, 2000.

[19] Noguchi, M., Kimoto, A., Gierse, J.K., Walker, M.C., Zweifel, B.S., Nozaki, K., and Sasamata, M.: Enzymologic and pharmacologic profile of loxoprofen sodium and its metabolites. *Biol. Pharm. Bull.*, **28**, 2075–2079, 2005.

[20] Mason, R.P., Walter, M.F., Day, C.A., and Jacob, R.F.: A biological rationale for the cardiotoxic effects of rofecoxib: comparative analysis with other COX-2 selective agents and NSAIDs. *Subcell. Biochem.*, **42**, 175–190, 2007.

[21] White, W.B., West, C.R., Borer, J.S., Gorelick, P.B., Lavange, L., Pan, S.X., Weiner, E., and Verburg, K.M.: Risk of cardiovascular events in patients receiving celecoxib: a meta-analysis of randomized clinical trials. *Am. J. Cardiol.*, **99**, 91–98, 2007.

[22] Silverstein, F.E., Faich, G., Goldstein, J.L., Simon, L.S., Pincus, T., Whelton, A., Makuch, R., Eisen, G., Agrawal, N.M., Stenson, W.F., Burr, A.M., Zhao, W.W., Kent, J.D., Lefkowith, J.B., Verburg, K.M., and Geis, G.S.: Gastrointestinal toxicity with celecoxib vs nonsteroidal anti-inflammatory drugs for osteoarthritis and rheumatoid arthritis: the CLASS study: A randomized controlled trial. Celecoxib Long-term Arthritis Safety Study. *J.A.M.A.*, **284**, 1247–1255, 2000.

Leukemia Research 34 (2010) 793–799

Contents lists available at ScienceDirect

Leukemia Research

journal homepage: www.elsevier.com/locate/leukres

Osteoclasts are involved in the maintenance of dormant leukemic cells

Asumi Yokota[a], Shinya Kimura[a,b,*], Ruriko Tanaka[a], Miki Takeuchi[a], Hisayuki Yao[a], Kazuki Sakai[a], Rina Nagao[a], Junya Kuroda[c], Yuri Kamitsuji[a], Eri Kawata[a], Eishi Ashihara[a], Taira Maekawa[a]

[a] Department of Transfusion Medicine and Cell Therapy, Kyoto University Hospital, Kyoto, Japan
[b] Department of Hematology, Respiratory Diseases and Oncology, Saga University Hospital, Saga City, Japan
[c] Division of Hematology and Oncology, Department of Medicine, Kyoto Prefectural University of Medicine, Kyoto, Japan

ARTICLE INFO

Article history:
Received 12 July 2009
Received in revised form 12 July 2009
Accepted 30 August 2009
Available online 24 September 2009

Keywords:
Osteoclasts
Osteoblasts
TGF-β_1
Bone marrow microenvironment

ABSTRACT

Osteoclasts (OCs) are specialized cells for the resorption of bone matrix that have also been recently reported to be involved in the mobilization of hematopoietic progenitor cells. When Ba/F3 cells expressing wild-type *bcr-abl* were co-cultured with osteoblasts (OBs), OCs, and bone slices, their proliferation was significantly suppressed, and the Ki-67 negative population, which is believed to be in G_0 phase, was increased. The results of our *in vitro* experiments suggest that OCs could be involved in the maintenance of dormant leukemic cells in the bone marrow (BM) microenvironment through the release of soluble factors, one of which could be TGF-β.

1. Introduction

It has been suggested that the bone marrow (BM) microenvironment might play an important role in regulating hematopoiesis, and is considered a hematopoietic stem cell (HSC) niche. HSCs are thought to reside in the BM niche and respond to various signals relayed by soluble factors, adherent molecules, or the extracellular matrix that regulate their self-renewal, proliferation, or differentiation. Osteoblasts (OBs) are bone-derived stromal cells that line the surface of the endosteum and mineralize the bone matrix. These cells are destined to form the HSC niche in the endosteum and regulate HSC number or differentiation [1–4]. It is also recognized that the HSC niche is a hypoxic environment, thus HSCs are protected from oxidative stress and are maintained in a senescent state in the niche [5,6]. Osteoclasts (OCs) are terminally differentiated cells of the monocyte/macrophage lineage that resorb mineralized bone matrix and degrade the extracellular matrix of the endosteum in trabecular bone. The direct interaction of OBs and OC precursors is essential for OC differentiation and is mediated by the binding of the RANK ligand (RANKL) on OBs to the receptor activator of NF-κB (RANK) on OC precursors [7–9]. Recently, both OBs and OCs have been reported to be involved in regulating hematopoiesis in the BM niche through the degradation of the niche components that anchor HSCs to the niche [10,11]. Another group has speculated that OCs induce the release of calcium ions from the bone matrix at the endosteum and the resulting calcium gradient directs calcium-sensing receptor (CaR)-expressing HSCs to engraft and localize to the BM niche [12]. We have previously reported that the third-generation bisphosphonate, zoledronic acid (ZOL), exerts anti-tumor effects in a murine model of chronic myelogenous leukemia (CML) [13–15]. ZOL induces apoptosis in OCs and is used as a therapeutic agent in the treatment of osteoporosis or hypercalcemia of malignancy. We hypothesized that ZOL suppresses the progression of leukemia not only by directly inducing apoptosis in leukemic cells, but also by reducing the number of OCs. To test this hypothesis, we investigated whether OCs influence the growth of leukemic cells by using an *in vitro* co-culture system. In the present study, we demonstrate that OCs suppress the growth of leukemic cells and induce a dormant state *in vitro*. We also present evidence that OCs might maintain leukemic cells in a quiescent state in the BM microenvironment which could act as both a normal hematopoietic and leukemic stem cell niche, potentially contributing to the incidence of relapse and the onset of acquired drug resistance in leukemias.

2. Materials and methods

2.1. Reagents and cell lines

Ba/F3 cells expressing wild-type (wt) *bcr-abl*^{p210} were generated as previously described [16]. Cells were maintained at 37 °C in a fully humidified atmosphere of 5% CO_2 as suspension cultures in RPMI-1640 medium (Wako, Osaka, Japan) supplemented with 10% heat-inactivated fetal bovine serum (FBS), 100 μg/mL

* Corresponding author at: Department of Hematology, Respiratory Diseases and Oncology, Saga University Hospital 1-1, 5 cho-me Nabeshima, Saga City, Saga 849-8501, Japan. Tel.: +81 952 34 2353; fax: +81 952 34 2017.
E-mail address: shkimu@cc.saga-u.ac.jp (S. Kimura).

0145-2126/$ – see front matter © 2009 Elsevier Ltd. All rights reserved.
doi:10.1016/j.leukres.2009.08.034

penicillin–streptomycin and 292 μg/mL L-glutamine (Gibco, Paisley, Scotland). Recombinant human TGF-β_1 and monoclonal anti-TGF-β antibody were purchased from R&D systems (Minneapolis, MN, USA). A Quantikine Mouse/Rat/Porcine/Canine TGF-β_1 immunoassay (R&D systems) was used for the detection of murine TGF-β_1 in culture supernatants.

2.2. Primary murine osteoblasts

Primary murine OBs were enzymatically isolated from the calvaria of 1–2-day-old BALB/cA mice (CLEA Japan, Osaka, Japan) by sequential digestion with 0.1% collagenase (Wako) and 0.2% dispase (Sanko Junyaku, Tokyo, Japan) solution. Harvested cells were plated in 100 mm dishes in alpha-MEM (Sigma–Aldrich, St. Louis, MO, USA) containing 10% heat-inactivated FBS, 100 μg/mL penicillin–streptomycin and 292 μg/mL L-glutamine. After incubation for 24 h, the culture medium was changed, and cells were collected on the subsequent day by trypsinization with 0.05% trypsin–EDTA (Invitrogen, Carlsbad, CA) and expanded. Six to seven days after the initial harvest, cells were collected and stored at −80 °C until use.

2.3. Osteoclast induction in vitro

BM cells were flushed out with 10% FBS alpha-MEM from both tibias and femurs of 5–10-week-old BALB/cA mice. Each well of a culture plate was coated with 500 μL of a mixture of collagen gel (Cellmatrix Type I-A, Nitta gelatin, Osaka, Japan), 5× alpha-MEM (GIBCO) and $NaHCO_3$/HEPES buffer following the manufacturer's instructions. First, bone slices derived from adult murine femurs were placed on the collagen gel. Next, OBs were seeded at a concentration of 1×10^5 cells/well, and then 2×10^6 cells/well of BM cells were seeded alongside the OBs. Vitamin D_3 (Calcitriol, Wako) and prostaglandin E_2 (Wako) were added to each well at a final concentration of 0.02 μM and 2 μM, respectively. Six to seven days after the start of co-culture, OBs and OCs were used for co-culture with Ba/F3 wt *bcr-abl* cells.

2.4. Indirect co-culture of leukemic cells with osteoblasts, osteoclasts and bone slices

Ba/F3 wt *bcr-abl* cells were seeded at 1×10^4 cells/well into transwell chambers (Transwell #3401, Corning Incorporated, Acton, MA, USA) in which the membrane pore size is 0.4 μm, thereby creating an indirect co-culture condition. Viable cells were counted by trypan blue dye exclusion at 48 and 72 h after the co-culture was initiated. At 72 h, co-cultured Ba/F3 wt *bcr-abl* cells were harvested and fixed with cold 70% ethanol, and stored at −20 °C until cell cycle analysis.

2.5. TRAP staining

Cells were fixed with 10% neutral buffered formaldehyde (Wako) at room temperature for 10 min and fixed again with ethanol–acetone (50:50, vol/vol) for 1 min. Cells were then incubated with the TRAP staining solution: 5 mg of naphthol AS-MX phosphate (Sigma) was dissolved in 0.5 mL of N,N-dimethyl formamide (Wako), and 30 mg of fast red violet LB salt (Sigma) and 0.1 M sodium acetate buffer, pH 5.0, containing 50 mM sodium tartrate, were added to the mixture. After incubation for 5 min at room temperature, cells were washed with diluted water.

2.6. Cell cycle analysis

Fixed Ba/F3 wt *bcr-abl* cells were washed twice with wash buffer (PBS containing 1% FBS) and the pellet was resuspended to a concentration of 1×10^6 cells/100 μL. 20 μL of FITC anti-human Ki-67 antibody or FITC isotype control (BD Pharmingen, San Diego, CA, USA) was added to 100 μL of cell suspension and incubated at room temperature for 30 min in the dark. Cells were then washed with wash buffer and resuspended in 500 μL of wash buffer, followed by the addition of 20 μL of BD Via-Probe™ Cell Viability Solution (BD Pharmingen). The samples were analyzed using FACSCanto II flow cytometer and BD FACSDiva software.

2.7. Western blot analysis

Protein samples were separated by sodium dodecyl sulfate-polyacrylamide gel electrophoresis and electroblotted onto a nitrocellulose membrane (GE Healthcare Bio-Sciences, Tokyo, Japan). The membranes were saturated with 5% (wt/vol) non-fat dry milk in TBST (25 mM Tris [tris(hydroxymethyl)aminomethane]–HCl, pH 7.8, 140 mM NaCl, 0.1% [vol/vol] Tween20), and incubated overnight at 4 °C with rabbit monoclonal anti-smad2/3 antibody (1:1000; Cell Signaling Technology, Danvers, MA, USA), rabbit monoclonal anti-phospho-smad2 (1:1000; Cell Signaling Technology), or rabbit monoclonal anti-actin antibodies (1:1000; Sigma). The membranes were washed thoroughly with TBST and incubated for 1 h at room temperature with anti-rabbit IgG coupled to horseradish peroxidase (1:1000; GE Healthcare Biosciences). Detection was performed with enhanced chemiluminescence kits (GE Healthcare Biosciences).

2.8. Measurement of TGF-β_1 in the culture supernatants by ELISA

The culture supernatants of OBs, OCs, and/or bone slices were collected and centrifuged for particle removal. Samples were stored at −80 °C until use. ELISA for murine TGF-β_1 was performed according to manufacturer's instructions. TGF-β_1 concentrations were calculated by subtracting the background of FBS in the supernatants from the actual values.

2.9. Statistical analysis

P values were derived from 2-sided tests, and values of less than 0.05 were considered statistically significant.

3. Results

3.1. OCs suppress the growth of Ba/F3 wt bcr-abl cells in the presence of bone slices

We indirectly co-cultured Ba/F3 wt *bcr-abl* cells with OBs, OCs, and/or bone slices using transwell chambers. As shown in Fig. 1A, OBs enhanced the growth of Ba/F3 wt *bcr-abl* cells ("OB") and this effect was observed even in the presence of OCs ("OB + OC"). Interestingly, when bone slices were added to the OB + OC well ("OB + OC + bone"), the proliferation of Ba/F3 wt *bcr-abl* cells was significantly suppressed compared to OB + OC. Thus, we hypothesized that OCs might suppress the proliferation of Ba/F3 wt *bcr-abl* cells through the activity of soluble factors that are released from the bone slices or produced in the presence of the bone slices by OCs. When Ba/F3 cells were cultured in the presence of bone slices alone, no increase in the proliferation rate was observed,

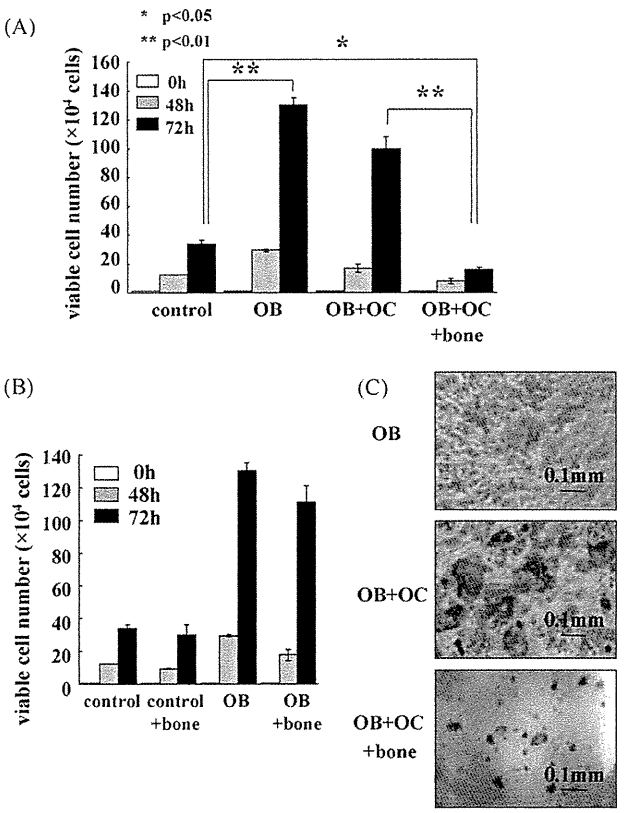

Fig. 1. OCs suppress the growth of Ba/F3 wt *bcr-abl* cells in the presence of bone slices. (A and B) Each bar indicates the viable cell number at 0 h (white), 48 h (gray) and 72 h (black) after the co-culture was initiated. The representative results shown are the means ± standard deviations (SD) of duplicated counts from two independent wells. (C) The images of TRAP-stained wells of OBs only, OB + OC, and OB + OC + bone 72 h after the co-culture were initiated.

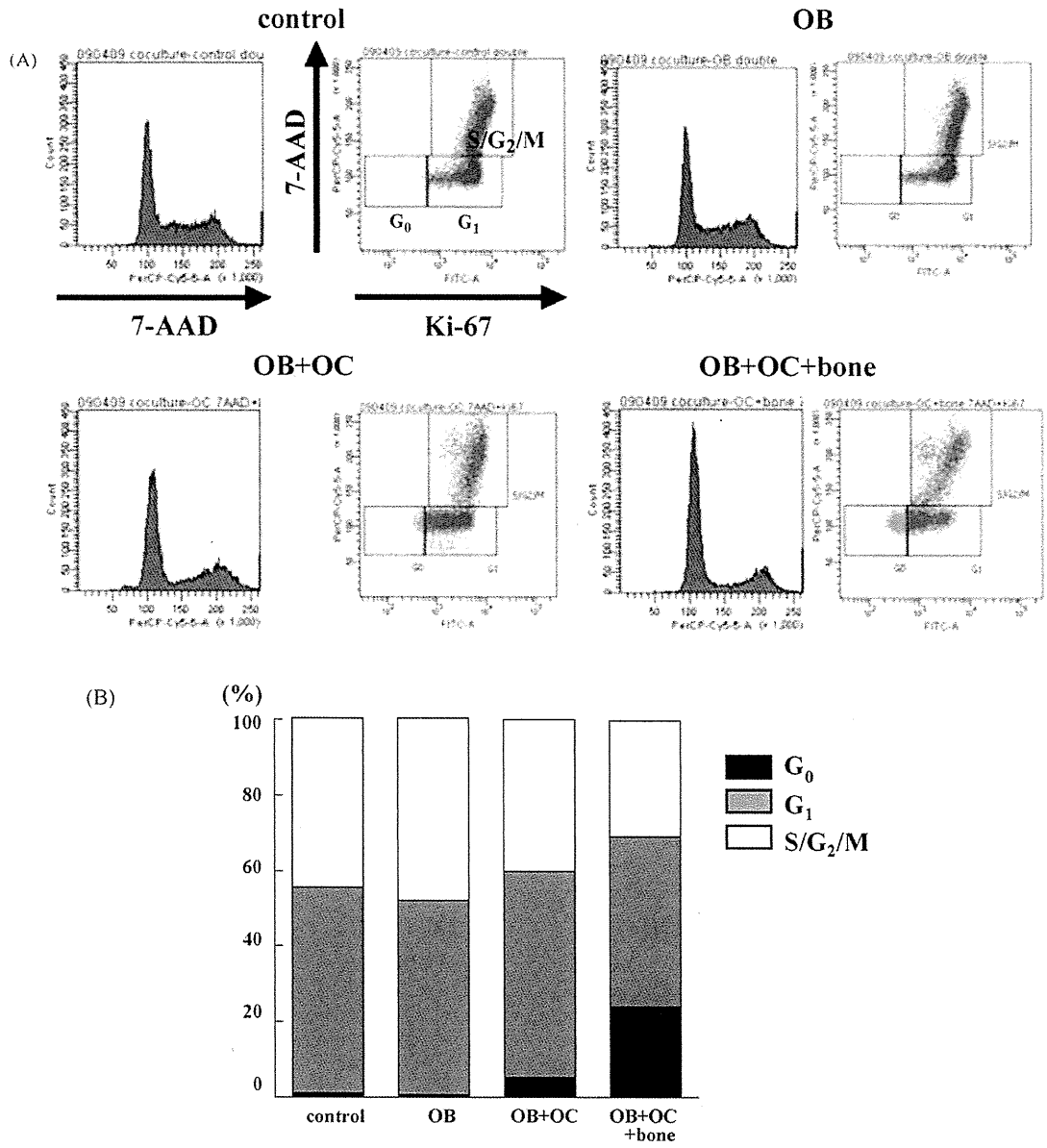

Fig. 2. OCs with bone slices increased the Ki-67-negative G_0 population in Ba/F3 wt *bcr-abl* cells. (A) Each figure shows representative data from three independent experiments. Co-cultured Ba/F3 wt *bcr-abl* cells were harvested 72 h after co-culture was initiated and were analyzed for their cell cycle status by flow cytometry following 7-AAD and Ki-67 staining. The percentages of cells in each cell cycle phase are shown in (B).

which confirms that the bone slices themselves did not influence the growth of Ba/F3 wt *bcr-abl* cells (Fig. 1B). Mature OCs identified by TRAP staining were observed in wells with OB+OC and OB+OC+bone, indicating that mature OCs were maintained in these co-culture experiments. In OB+OC+bone wells, $TRAP^+$ OCs were also observed on the bone slices (Fig. 1C).

3.2. OCs induced Ki-67-negative population in leukemic cells

We next sought to determine the source of growth suppression of Ba/F3 wt *bcr-abl* cells in the OB+OC+bone co-culture. First, we examined the cell cycle status of Ba/F3 wt *bcr-abl* cells co-cultured with OBs, OCs and/or bone slices. Ki-67 is expressed throughout all the cell cycle phases except G_0, thus 7-AAD and Ki-67 staining can distinguish cells in G_0 from those in G_0/G_1 by flow cytometry [17]. Interestingly, compared to the OB+OC co-culture, cells in the OB+OC+bone co-culture had an obviously increased Ki-67-negative population, which indicates resting cells in G_0 phase (Fig. 2A and B).

3.3. Effect of TGF-β_1 released or produced in the presence of bone slices on the growth of leukemic cells

Recently, TGF-β_1 was reported to be important for the maintenance of HSCs in the quiescent state in the BM niche [18]. TGF-β is also one of the major cytokines that accumulate in the bone matrix [19–21]. We speculated that OCs might suppress the growth of leukemic cells through the production or release of TGF-β_1 from the bone slices in our co-culture experiments. Thus, we used ELISA to measure the levels of TGF-β_1 in the culture supernatants. TGF-β_1 was significantly higher in supernatants from the OB+OC+bone co-culture than in supernatants from OB or OB+OC co-cultures (Fig. 3A), which suggests that OCs facilitate the release of TGF-β_1 from the bone slices. Next, we added an anti-TGF-β antibody

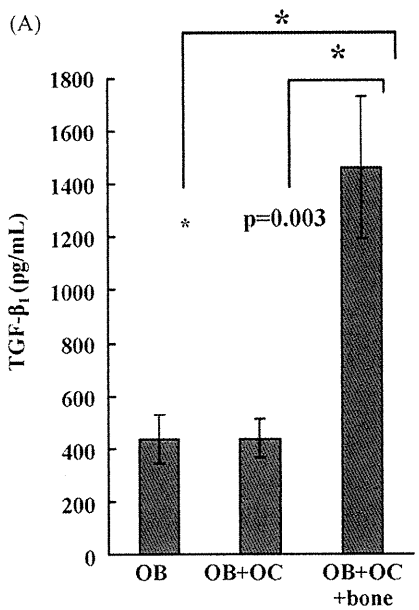

(C)

	G_0	G_1	$S/G_2/M$
control	1.0	50.5	47.7
Ab	0.6	52.8	45.7
OB	0.7	55.0	43.6
OB+Ab	0.9	48.2	48.3
OB+OC	0.8	50.2	45.1
OB+OC+Ab	0.7	54.3	44.5
OB+OC+bone	6.8	60.7	31.7
OB+OC+bone+Ab	3.8	61.4	34.7

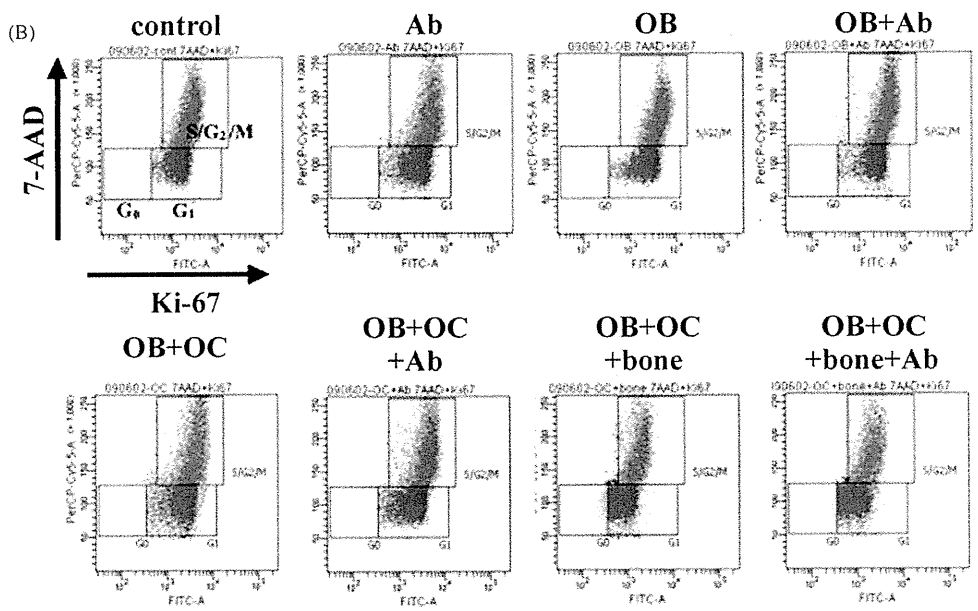

Fig. 3. TGF-β_1 released from the bone slices might affect the growth of Ba/F3 wt *bcr-abl* cells. (A) TGF-β_1 concentrations in the supernatants of OB, OB + OC, and OB + OC + bone were measured by ELISA. The results shown are the means ± SD of three independent experiments in duplicate. (B and C) 1 μg/mL of anti-TGF-β antibody was added to each co-culture condition. Cell cycle status of Ba/F3 wt *bcr-abl* cells after 72 h of co-culture was analyzed by flow cytometry following Ki-67 and 7-AAD staining. Representative results of three independent experiments are shown.

to the transwells. Addition of the anti-TGF-β antibody reduced the Ki-67-negative G_0 population in OB + OC + bone cells (Fig. 3B). These results suggest that the growth suppressive effect observed in the OB + OC + bone co-culture might be yielded, in part, via TGF-β_1.

Finally, we examined whether exogenous TGF-β_1 could increase the Ki-67-negative G_0 population in Ba/F3 wt *bcr-abl* cells. We treated Ba/F3 wt *bcr-abl* cells with various concentrations of recombinant TGF-β_1 and/or anti-TGF-β antibody. TGF-β_1 suppressed the growth of Ba/F3 wt *bcr-abl* cells and slightly increased the Ki-67-negative population, while the addition of the anti-TGF-β antibody completely suppressed this effect (Fig. 4A–C). We confirmed that the TGF-β antibody inhibited the phosphorylation of Smad2, a major signaling molecule of the TGF-β pathway (Fig. 4D). Therefore, it appears that the TGF-β antibody might reduce the dormant Ki-67-negative Ba/F3 population in the co-culture experiments through inhibition of the TGF-β pathway.

4. Discussion

Leukemic cells have been suggested to interact closely with the BM microenvironment [22]. It is believed that in this environment they receive various signals that are able to protect the leukemic cells from apoptosis induced by anti-cancer drugs and promote their survival or proliferation [23–27]. The BM microenvironment has also been implicated in the induction of myeloproliferative syn-

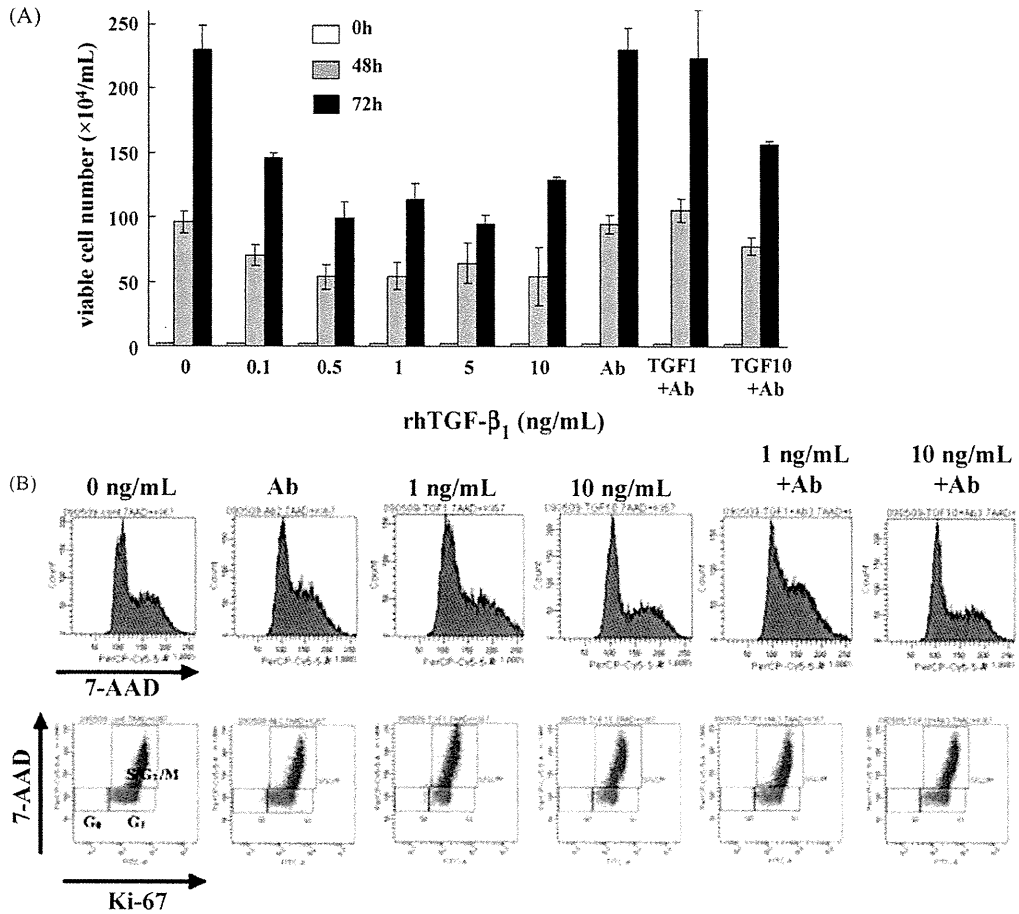

TGF-β1 (ng/mL)	G_0	G_1	$S/G_2/M$
0	1.2	49.2	50.3
1	2.2	42.3	56.3
10	1.5	50.6	48.4
Ab	2.3	46.7	51.4
1+Ab	0.8	42.4	57.6
10+Ab	1.0	50.0	49.5

Fig. 4. TGF-β_1 might maintain Ba/F3 wt *bcr-abl* cells in a dormant state. (A) Ba/F3 wt *bcr-abl* cells were treated with the indicated doses of TGF-β_1 for 72 h. The number of viable cells was counted by trypan blue staining, and (B) cell cycle analysis was performed by flow cytometry following 7-AAD and Ki-67 staining. The percentage of cells in each cell cycle phase is shown in (C). (D) Western blot analysis shows that recombinant TGF-β_1 induced phosphorylation of Smad protein, and addition of TGF-β antibody inhibited this phosphorylation in Ba/F3 wt *bcr-abl* cells.

drome through interaction with hematopoietic cells [28,29], and it was reported that leukemic cells influence the BM niche and disrupt normal hematopoiesis [30]. Recently, OCs have been shown to play a role in the mobilization of hematopoietic progenitor cells through matrix metalloproteinase-9 or cathepsin-K mediated cleavage of stromal cell-derived factor-1 (SDF-1) or stem cell factor (SCF), which anchor HSCs to the BM niche [10]. In this study, we hypothesized that the anti-tumor activity of ZOL observed in previous studies was due to a reduction in the number of mature OCs in the BM microenvironment. In cases of breast cancer [31] or prostate cancer [32] that metastasize to the bones, or in multiple myeloma [33], the close interaction between OCs and tumor cells is believed to be important for tumor progression or survival in the local microenvironment. The tumor cells activate OCs and induce bone-resorption activity, thereby increasing the available growth area and stimulating the release of growth factors from the bone matrix. Thus, it is possible that the survival or proliferation of leukemic cells is enhanced by the activity of OCs in the BM microenvironment.

Recently, it was reported that TGF-β might induce HSC hibernation in the BM niche [18]. TGF-β signaling plays an important role in the regulation of normal hematopoiesis by preventing progression through the cell cycle and promoting differentiation [34–36]. In acute myelogenous leukemia (AML) or CML, impairment of the negative growth-regulatory effects exerted by TGF-β signaling has been reported to contribute to the transformation, persistence, and maintenance of leukemic clones, and also to the development of drug resistance in leukemic cells [37–39].

In our co-culture experiments, OCs were able to increase the population of Ki-67-negative dormant leukemic cells only in the

presence of bone slices, and higher levels of TGF-β_1 were detected in the supernatants of cells in the OB + OC + bone co-culture. Therefore, it appears that OCs might maintain leukemic cells in a quiescent state in the BM microenvironment through the release of TGF-β. Quiescence is also likely to be important for the survival of leukemia-initiating cells (LICs) or leukemia stem cells (LSCs) [40,41]. Thus, these quiescent cells in the BM niche could become effective targets for the treatment of leukemia [42]. Our data suggests that TGF-β released or produced in the BM niche by OCs might contribute to the maintenance of quiescent LIC or LSC populations.

However, it remains unclear why OB + OC + bone could increase the Ki-67-negative G_0 population more strongly than recombinant TGF-β_1. One possible explanation is that other cytokines produced or released in OB + OC + bone co-culture in addition to TGF-β_1 regulate the proliferation of leukemic cells and work synergistically with TGF-β_1. Another possibility is that TGF-β_1 might induce the production of other soluble factors that affect the cell cycle progression of leukemic cells by OCs. Further experiments are necessary to better define the mechanism by which OCs and TGF-β_1 are able to influence the growth of leukemic cells.

5. Conclusion

In conclusion, our data indicates that OCs might represent a novel target for the development of therapies that target dormant leukemic cells in the BM microenvironment, thereby potentially reducing the incidence of relapse and the onset of acquired drug resistance in leukemic diseases.

Conflict of interest statement

The authors report no potential conflicts of interest.

Acknowledgements

We gratefully thank Prof. Naoyuki Takahashi and Prof. Nobuyuki Udagawa, Matsumoto Dental University, for technical advice, and Yoko Nakagawa for her excellent technical support. This work was supported by a Grant-in-Aid for Japan Society for the Promotion of Science (JSPS) Fellows.

Contributions. Asumi Yokota, Shinya Kimura, Eishi Ashihara and Taira Maekawa designed research; Asumi Yokota, Ruriko Tanaka, Miki Takeuchi, Yao Hisayuki, Kazuki Sakai, Rina Nagao, Junya Kuroda, Yuri Kamitsuji, Eri Kawata and Eishi Ashihara performed research; Asumi Yokota and Shinya Kimura analyzed data; Asumi Yokota, Shinya Kimura and Taira Maekawa wrote the paper.

References

[1] Calvi LM, Adams GB, Weibrecht KW, Weber JM, Olson DP, Knight MC, et al. Osteoblastic cells regulate the haematopoietic stem cell niche. Nature 2003;425:841–6.
[2] Zhang J, Niu C, Ye L, Huang H, He X, Tong WG, et al. Identification of the haematopoietic stem cell niche and control of the niche size. Nature 2003;425:836–41.
[3] Arai F, Hirao A, Ohmura M, Sato H, Matsuoka S, Takubo K, et al. Tie2/angiopoietin-1 signaling regulates hematopoietic stem cell quiescence in the bone marrow niche. Cell 2004;118:149–61.
[4] Yoshihara H, Arai F, Hosokawa K, Hagiwara T, Takubo K, Nakamura Y, et al. Thrombopoietin/MPL signaling regulates hematopoietic stem cell quiescence and interaction with the osteoblastic niche. Cell Stem Cell 2007;1:685–97.
[5] Hosokawa K, Arai F, Yoshihara H, Nakamura Y, Gomei Y, Iwasaki H, et al. Function of oxidative stress in the regulation of hematopoietic stem cell–niche interaction. Biochem Biophys Res Commun 2007;363:578–83.
[6] Kubota Y, Takubo K, Suda T. Bone marrow long label-retaining cells reside in the sinusoidal hypoxic niche. Biochem Biophys Res Commun 2008;366:335–9.
[7] Takahashi N, Akatsu T, Udagawa N, Sasaki T, Yamaguchi A, Moseley JM, et al. Osteoblastic cells are involved in osteoclast formation. Endocrinology 1988;123:2600–2.
[8] Lacey DL, Timms E, Tan HL, Kelley MJ, Dunstan CR, Burgess T, et al. Osteoprotegerin ligand is a cytokine that regulates osteoclast differentiation and activation. Cell 1998;93:165–76.
[9] Boyle WJ, Simonet WS, Lacey DL. Osteoclast differentiation and activation. Nature 2003;423:337–42.
[10] Kollet O, Dar A, Shivtiel S, Kalinkovich A, Lapid K, Sztainberg Y, et al. Osteoclasts degrade endosteal components and promote mobilization of hematopoietic progenitor cells. Nat Med 2006;12:657–64.
[11] Shivtiel S, Kollet O, Lapid K, Schajnovitz A, Goichberg P, Kalinkovich A, et al. CD45 regulates retention, motility, and numbers of hematopoietic progenitors, and affects osteoclast remodeling of metaphyseal trabecules. J Exp Med 2008;205:2381–95.
[12] Adams GB, Chabner KT, Alley IR, Olson DP, Szczepiorkowski ZM, Poznansky MC, et al. Stem cell engraftment at the endosteal niche is specified by the calcium-sensing receptor. Nature 2006;439:599–603.
[13] Kuroda J, Kimura S, Segawa H, Kobayashi Y, Yoshikawa T, Urasaki Y, et al. The third-generation bisphosphonate zoledronate synergistically augments the anti-Ph+ leukemia activity of imatinib mesylate. Blood 2003;102:2229–35.
[14] Kimura S, Kuroda J, Segawa H, Sato K, Nogawa M, Yuasa T, et al. Antiproliferative efficacy of the third-generation bisphosphonate, zoledronic acid, combined with other anticancer drugs in leukemic cell lines. Int J Hematol 2004;79:37–43.
[15] Segawa H, Kimura S, Kuroda J, Sato K, Yokota A, Kawata E, et al. Zoledronate synergises with imatinib mesylate to inhibit Ph primary leukaemic cell growth. Br J Haematol 2005;130:558–60.
[16] Kimura S, Naito H, Segawa H, Kuroda J, Yuasa T, Sato K, et al. NS-187, a potent and selective dual Bcr-Abl/Lyn tyrosine kinase inhibitor, is a novel agent for imatinib-resistant leukemia. Blood 2005;106:3948–54.
[17] van Pelt K, de Haan G, Vellenga E, Daenen SM. Administration of low-dose cytarabine results in immediate S-phase arrest and subsequent activation of cell cycling in murine stem cells. Exp Hematol 2005;33:226–31.
[18] Yamazaki S, Iwama A, Takayanagi S, Eto K, Ema H, Nakauchi H. TGF-beta as a candidate bone marrow niche signal to induce hematopoietic stem cell hibernation. Blood 2009;113:1250–6.
[19] Seyedin SM, Thomas TC, Thompson AY, Rosen DM, Piez KA. Purification and characterization of two cartilage-inducing factors from bovine demineralized bone. Proc Natl Acad Sci USA 1985;82:2267–71.
[20] Centrella M, Canalis E. Transforming and nontransforming growth factors are present in medium conditioned by fetal rat calvariae. Proc Natl Acad Sci USA 1985;82:7335–9.
[21] Seyedin SM, Thompson AY, Bentz H, Rosen DM, McPherson JM, Conti A, et al. Cartilage-inducing factor-A. Apparent identity to transforming growth factor-beta. J Biol Chem 1986;261:5693–5.
[22] Lane SW, Scadden DT, Gilliland DG. The leukemic stem cell niche—current concepts and therapeutic opportunities. Blood 2009.
[23] Matsunaga T, Takemoto N, Sato T, Takimoto R, Tanaka I, Fujimi A, et al. Interaction between leukemic-cell VLA-4 and stromal fibronectin is a decisive factor for minimal residual disease of acute myelogenous leukemia. Nat Med 2003;9:1158–65.
[24] Ishikawa F, Yoshida S, Saito Y, Hijikata A, Kitamura H, Tanaka S, et al. Chemotherapy-resistant human AML stem cells home to and engraft within the bone-marrow endosteal region. Nat Biotechnol 2007;25:1315–21.
[25] Ninomiya M, Abe A, Katsumi A, Xu J, Ito M, Arai F, et al. Homing, proliferation and survival sites of human leukemia cells in vivo in immunodeficient mice. Leukemia 2007;21:136–42.
[26] Fleming HE, Janzen V, Lo Celso C, Guo J, Leahy KM, Kronenberg HM, et al. Wnt signaling in the niche enforces hematopoietic stem cell quiescence and is necessary to preserve self-renewal in vivo. Cell Stem Cell 2008;2:274–83.
[27] Jin L, Tabe Y, Konoplev S, Xu Y, Leysath CE, Lu H, et al. CXCR4 up-regulation by imatinib induces chronic myelogenous leukemia (CML) cell migration to bone marrow stroma and promotes survival of quiescent CML cells. Mol Cancer Ther 2008;7:48–58.
[28] Walkley CR, Olsen GH, Dworkin S, Fabb SA, Swann J, McArthur GA, et al. A microenvironment-induced myeloproliferative syndrome caused by retinoic acid receptor gamma deficiency. Cell 2007;129:1097–110.
[29] Walkley CR, Shea JM, Sims NA, Purton LE, Orkin SH. Rb regulates interactions between hematopoietic stem cells and their bone marrow microenvironment. Cell 2007;129:1081–95.
[30] Colmone A, Amorim M, Pontier AL, Wang S, Jablonski E, Sipkins DA. Leukemic cells create bone marrow niches that disrupt the behavior of normal hematopoietic progenitor cells. Science 2008;322:1861–5.
[31] Cicek M, Oursler MJ. Breast cancer bone metastasis and current small therapeutics. Cancer Metastasis Rev 2006;25:635–44.
[32] Bradley DA, Hussain M, Dipaola RS, Kantoff P. Bone directed therapies for prostate cancer. J Urol 2007;178:S42–8.
[33] Silvestris F, Lombardi L, De Matteo M, Bruno A, Dammacco F. Myeloma bone disease: pathogenetic mechanisms and clinical assessment. Leuk Res 2007;31:129–38.
[34] Chadwick K, Shojaei F, Gallacher L, Bhatia M. Smad7 alters cell fate decisions of human hematopoietic repopulating cells. Blood 2005;105:1905–15.
[35] Larsson J, Karlsson S. The role of Smad signaling in hematopoiesis. Oncogene 2005;24:5676–92.
[36] Chabanon A, Desterke C, Rodenburger E, Clay D, Guerton B, Boutin L, et al. A cross-talk between stromal cell-derived factor-1 and transforming growth factor-beta controls the quiescence/cycling switch of CD34(+) progenitors through FoxO3 and mammalian target of rapamycin. Stem Cells 2008;26:3150–61.

[37] Atfi A, Abecassis L, Bourgeade MF. Bcr-Abl activates the AKT/Fox O3 signalling pathway to restrict transforming growth factor-beta-mediated cytostatic signals. EMBO Rep 2005;6:985–91.
[38] Dong M, Blobe GC. Role of transforming growth factor-beta in hematologic malignancies. Blood 2006;107:4589–96.
[39] Moller GM, Frost V, Melo JV, Chantry A. Upregulation of the TGFbeta signalling pathway by Bcr-Abl: implications for haemopoietic cell growth and chronic myeloid leukaemia. FEBS Lett 2007;581:1329–34.
[40] Jordan CT, Guzman ML. Mechanisms controlling pathogenesis and survival of leukemic stem cells. Oncogene 2004;23:7178–87.
[41] Ito K, Bernardi R, Morotti A, Matsuoka S, Saglio G, Ikeda Y, et al. PML targeting eradicates quiescent leukaemia-initiating cells. Nature 2008;453:1072–8.
[42] Elrick LJ, Jorgensen HG, Mountford JC, Holyoake TL. Punish the parent not the progeny. Blood 2005;105:1862–6.

OPEN ACCESS Freely available online

PLoS one

Noninvasive Tracking of Donor Cell Homing by Near-Infrared Fluorescence Imaging Shortly after Bone Marrow Transplantation

Takashi Ushiki[1,2], Shinae Kizaka-Kondoh[1]*, Eishi Ashihara[3], Shotaro Tanaka[1¤], Masayoshi Masuko[2], Hideyo Hirai[3], Shinya Kimura[4], Yoshifusa Aizawa[5], Taira Maekawa[3], Masahiro Hiraoka[1]

1 Department of Radiation Oncology and Image-Applied Therapy, Kyoto University Graduate School of Medicine, Kyoto, Japan, **2** Department of Hematology, Niigata University Graduate School of Medical and Dental Sciences, Niigata, Japan, **3** Department of Transfusion Medicine and Cell Therapy, Kyoto University Hospital, Kyoto, Japan, **4** Department of Internal Medicine, Faculty of Medicine, Saga University, Saga, Japan, **5** Department of Cardiology, Niigata University Graduate School of Medical and Dental Sciences, Niigata, Japan

Abstract

Background: Many diseases associated with bone marrow transplantation (BMT) are caused by transplanted hematopoietic cells, and the onset of these diseases occurs after homing of donor cells in the initial phase after BMT. Noninvasive observation of donor cell homing shortly after transplantation is potentially valuable for improving therapeutic outcomes of BMT by diagnosing the early stages of these diseases.

Methodology/Principal Findings: Freshly harvested near-infrared fluorescence-labeled cells were noninvasively observed for 24 h after BMT using a photon counting device to track their homing process. In a congenic BMT model, the homing of Alexa Fluor 750-labeled donor cells in the tibia was detected less than 1 h after BMT. In addition, subsequent cell distribution in an intraBM BMT model was successfully monitored for the first time using this method. In the allogeneic BMT model, T-cell depletion decreased the near-infrared fluorescence (NIRF) signals of the reticuloendothelial system.

Conclusions/Significance: This approach in several murine BMT models revealed that the transplanted cells homed within 24 h after transplantation. NIRF labeling is useful for tracking transplanted cells in the initial phase after BMT, and this approach can contribute to in vivo studies aimed at improving the therapeutic outcomes of BMT.

Citation: Ushiki T, Kizaka-Kondoh S, Ashihara E, Tanaka S, Masuko M, et al. (2010) Noninvasive Tracking of Donor Cell Homing by Near-Infrared Fluorescence Imaging Shortly after Bone Marrow Transplantation. PLoS ONE 5(6): e11114. doi:10.1371/journal.pone.0011114

Editor: Joshua Z. Rappoport, University of Birmingham, United Kingdom

Received March 17, 2010; **Accepted** May 24, 2010; **Published** June 14, 2010

Funding: This work was supported in part by a Grant-in-Aid for Scientific Research on Priority Areas, Cancer, from the Ministry of Education, Culture, Sports, Science and Technology, Japan (http://www.mext.go.jp/english/). The funders had no role in study design, data collection and analysis, decision to publish, or preparation of the manuscript.

Competing Interests: The authors have declared that no competing interests exist.

* E-mail: skondoh@kuhp.kyoto-u.ac.jp

¤ Current address: Department of Biochemistry, School of Medicine, Tokyo Women's Medical University, Tokyo, Japan

Introduction

Bone marrow transplantation (BMT) is an important procedure for curing hematological malignancies, although engraftment failure [1] and graft-versus-host disease (GVHD) [2] remain serious complications following allogeneic BMT. To examine these complications, it is important to monitor the transplanted donor cells in the initial phase after BMT because donor cell homing is a rapid process. Homing is defined as the anchoring of hematopoietic cells in their niche before cell proliferation [3]. Results of a colony-forming assay revealed that donor cell homing occurs within minutes or a few hours, rather than days, after BMT [4]. BMT-associated complications are suspected to begin just after homing of the donor cells; for example, in studies of engraftment failure, homing of hematopoietic stem cells (HSCs) is crucial and is the first step in hematopoietic reconstitution [5]. In acute GVHD (aGVHD), T-cell activation by host antigen-presenting cells [6,7] begins after homing in the reticuloendothelial system, and this process starts within a few days after BMT in murine GVHD models [8].

Recent molecular imaging techniques have facilitated significant advances in noninvasive optical imaging [9], which enable tracking of transplanted hematopoietic cells with greater accuracy in vivo. Bioluminescence imaging can precisely analyze the processes during BMT [10]. However, until now, bioluminescence imaging has provided sparse spatiotemporal information for donor cell homing in the initial phase after BMT.

In this study, we directly labeled donor BM cells using a near-infrared fluorescence (NIRF) dye with high tissue permeability and monitored the homing of transplanted cells shortly after BMT using a noninvasive whole-body imaging device IVIS-Spectrum. The overall results provide information regarding the homing of donor cells after BMT and intraBM-BMT (IBM-BMT), and the onset of GVHD. Noninvasive tracking of transplanted donor cells in the initial phase after BMT enables acquisition of spatiotemporal information regarding HSC homing, which can help identify

factors supporting HSC homing and mechanisms of hematopoietic reconstitution.

Materials and Methods

Ethics statement

All animal experiments in this study were performed with the approval of the Animal Experiment Committees of Kyoto University, Graduate School of Medicine. The approval number of the experiment is Med Kyo 09247. Approved experiments included use of transgenic mice and primary cells, cell transplantation, in vivo and ex vivo optical imaging, and UV irradiation.

Mice

Balb/c nu/nu (H-2^d, Thy 1.2), Balb/c (H-2^d, Thy 1.2), C57BL/6 (H-2^b, Thy 1.2), and FVB/N (H-2^q, Thy 1.1) mice were purchased from Japan SLC Inc. (Hamamatsu, Japan). Enhanced green fluorescent protein (EGFP) transgenic mice were generated by injecting the CAAG-EGFP expression vector into a one-cell embryo of an ICR closed colony (ICR/EGFP) [11], followed by breeding in an SPF animal facility. All mice were 7–9 weeks of age and were fasted according to our original fasting protocol from the day before BMT until 24 h after BMT (Supplemental Fig. S1) for suppression of autofluorescence from food particles in the gastrointestinal (GI) tract.

Cell preparation for transplantation and in vitro assays

BM cells were prepared from the medullary cavities of the humerus, femur, and tibia. Splenocytes were prepared by homogenization of the spleen. BM mononuclear cells (BM-MNCs) and spleen mononuclear cells (Sp-MNCs) were obtained by density gradient centrifugation using Lympholyte-M solution (Cedarlane Labs, Hornby, ON, Canada). T-cell-depleted (TCD) BM-MNCs were obtained by negative selection using Thy1.2^+ microbeads (Miltenyi Biotech, Auburn, CA, USA).

NIRF and 5-(6)-carboxyfluorescein diacetate succinimidyl ester (CFSE) labeling

Cy5.5 monofunctional dye (peak excitation: 675 nm, peak emission: 694 nm; GE Healthcare UK Ltd, Buckinghamshire, UK) and Alexa Fluor 750 carboxylic acid, succinimidyl ester (AF750) (peak excitation: 749 nm, peak emission: 775 nm; Invitrogen, Eugene, OR, USA) were dissolved in N, N-dimethylformamide. To prepare Cy5.5- or AF750-labeled cells, BM-MNCs and Sp-MNCs were incubated with Cy5.5 (0.4 mg/mL) or AF750 (0.1 mg/mL) for 15 min at 37°C under 5% CO_2. The cells were washed twice with phosphate-buffered saline (PBS) and then once with 10 mM Tris in PBS to disturb the active groups. For CFSE (Invitrogen) labeling, the cells were incubated in 5 μM CFSE in PBS for 10 min at 37°C, followed by washing with excess ice-cold PBS on ice for 5 min to quench staining. The cells were then washed 3 times with PBS. To prepare CFSE and NIRF double-positive cells, CFSE staining was performed before NIRF labeling.

Cell proliferation assays

NIRF-labeled Sp-MNCs (1×10^5) were seeded in a 96-well plate with 100 μL of phenol red-free RPMI 1640 (Wako Pure Chemical Industries Ltd., Osaka, Japan) supplemented with 1 mM sodium pyruvate, 10 mM HEPES, 100 units/mL penicillin, 100 μg/mL streptomycin, 50 μM mercaptoethanol, and 10% FCS. To stimulate splenocyte proliferation, recombinant mouse IL-2 (mIL-2) (20 ng/mL; R&D Systems, Minneapolis, MN, USA) and anti-CD3/CD28 antibody-coated beads (Dynabeads mouse CD3/CD28 T-cell expander; Invitrogen Dynal AS, Oslo, Norway) were added to the medium. The CD3/CD28 T-cell expander was used at a 1:1 bead-to-cell ratio according to the manufacturer's instructions. The viable cell number was analyzed as previously described [12] with slight modifications. The absorbance (450 nm) was measured 3 h after adding the cell-counting reagent.

Analysis of clonogenic myeloid and erythroid progenitors

BM cells (2×10^4) were harvested from 6- to 8-week-old Balb/c nu/nu mice and cultured in Methocult GF M3434 (Stem Cell Technologies, Vancouver, BC, Canada) according to the manufacturer's instructions after NIRF labeling. Granulocyte-macrophage colony-forming units (GM-CFUs); erythroid burst-forming units (BFU-Es); and granulocyte, erythrocyte, macrophage, and megakaryocyte colony-forming units (GEMM-CFUs) were scored after 7 days in culture.

Fluorescence-activated cell sorter (FACS) analyses

FACS data were obtained using a Canto II flow cytometer (Becton Dickinson, Mountain View, CA, USA) and analyzed using FACSDiva (Becton Dickinson) or FlowJo software (TreeStar, Ashland, OR, USA). A red helium-neon (633 nm) laser was used for excitation of Cy5.5 (analyzed using an APC filter) and AF750 (analyzed using an APC-Cy7 filter). NIRF-labeled ICR/EGFP BM-MNCs were used for analysis of chimerism of transplanted cells. Antibodies against FITC-conjugated Thy1.1 (CD90.1) and PE-conjugated Thy1.2 (CD90.2) were purchased from BD Pharmingen, San Diego, CA, USA. AF750-labeled Balb/c Thy1.2^+ cells (1×10^6) were mixed with unlabeled FVB/N Thy1.1^+ cells (1×10^6) in a 1:1 ratio and incubated together in PBS at 37°C for 3 h, and the AF750 intensity of Thy1.1^+ and Thy1.2^+ cells was determined. We estimated the percentages of EGFP$^+$ cells in the tibiae and peripheral blood of the recipients at 24, 48, and 72 h after BMT. Erythrocytes were removed using ACK lysis buffer (Invitrogen). DNA content was analyzed as previously described [13].

Pathological examinations

For ex vivo analyses of the chimerism of transplanted EGFP$^+$ cells in the tibiae, the recipient mice were sacrificed at 24, 48, or 72 h after BMT. BM cells were flushed from the tibiae using PBS and dyed with 100 μg/mL DAPI (Sigma-Aldrich, St. Louis, MO, USA). These cells were then observed with an inverted fluorescent microscope. To detect EGFP$^+$ cells in the organs after BMT, the Balb/c nu/nu mice receiving ICR/EGFP BM-MNCs were sacrificed at 24, 48, or 72 h after BMT. Organs from the mice were then removed, fixed in 10% formalin, and embedded in paraffin. Furthermore, 3-μm-thick sections were deparaffinized and incubated with blocking solution (1% Block Ace; Dainippon Pharmaceutical Co. Ltd., Osaka, Japan) for 15 min at room temperature. Sections were incubated with polyclonal rabbit anti-EGFP antibody (1:1000 dilution in PBS; Abcam, Cambridge, MA, USA) at 4°C overnight and then with FITC-conjugated swine anti-rabbit immunoglobulin (1:30 dilution in PBS; Dako, Glostrup, Denmark) for 1 h at room temperature. They were then washed and mounted in VECTASHIELD with DAPI (Vector Laboratories, Burlingame, CA, USA). All photos were taken using a BZ-9000 microscope (KEYENCE, Osaka, Japan).

Transplantation of donor cells

Balb/c nu/nu mice (7–9 weeks old) or Balb/c mice (7–9 weeks old) were lethally irradiated (8 Gy) in a single fraction by a ^{137}Cs γ-ray using a Gammacell 40 Exactor (MDS Nordion International

Inc., Ontario, Canada). BM-MNCs and Sp-MNCs were injected into the recipient mice through the tail vein at 6–8 h after irradiation. For ex vivo analyses of the chimerism of transplanted $EGFP^+$ cells in the tibiae or peripheral blood, 1×10^7 Cy5.5- or AF750-labeled ICR/EGFP BM-MNCs were transplanted into the Balb/c nu/nu mice. The recipient mice were sacrificed at 24, 48, or 72 h. For in vivo imaging with congenic BMT, 1×10^7 AF750-labeled Balb/c nu/nu BM-MNCs were injected into the Balb/c nu/nu mice. For allogeneic BMT, 1×10^7 AF750-labeled C57BL/6 BM-MNCs, 1×10^7 AF750-labeled TCD C57BL/6 BM-MNCs, or 5×10^6 AF750-labeled C57BL/6 TCD BM-MNCs plus 5×10^6 AF750-labeled C57BL/6 Sp-MNCs were injected into 7- to 9-week-old Balb/c nu/nu mice.

IBM-BMT model

IBM-BMT was performed as described previously [14]. In brief, 7- to 9-week-old Balb/c nu/nu mice were lethally irradiated (8 Gy) in a single fraction by a ^{137}Cs γ-ray 24 h before BMT. For IBM-BMT, the mice were then anesthetized with isoflurane, and the left tibia was gently drilled using a 26-G microsyringe (50 μL; Hamilton, Reno, NV, USA) through the patellar tendon. The AF750-labeled BM-MNCs (1×10^7 in 30 μL PBS) were directly injected into the BM cavity thereafter.

In vivo and ex vivo imaging of transplanted mice

In vivo imaging was performed using an IVIS Spectrum system (Xenogen, Alameda, CA, USA) at 5, 15, or 30 min and 1, 3, 6, 12, 18, or 24 h after BMT. During imaging, the mice were kept on the imaging stage under anesthesia with 2.5% isoflurane gas in oxygen flow (2 L/min). Transplanted Cy5.5- or AF750-labeled cells were detected using emission and excitation filters (excitation/emission: 640/700 for Cy5.5-labeled cells, 710/780 for AF750-labeled cells). The conditions were as follows: exposure time = 5 s, lamp level = high, binning = medium, field of view = 12.9×12.9 cm, and f/stop = 1. Ex vivo imaging was performed using the IVIS Spectrum system 24 h after BMT, under the same conditions as for in vivo imaging. For free NIRF injection, free Cy5.5 (625 ng) or AF750 (40 ng) in 100 μL Tris in PBS (10 mM), with the same fluorescence intensity as 1×10^7 NIRF BM-MNCs, was injected through the tail vein.

Statistical analysis

Student's *t* tests were used to determine the statistical significance. $P<0.05$ was considered significant.

Results

Direct NIRF labeling technique shows low cytotoxicity

Since most diseases associated with BMT are caused by transplanted hematopoietic cells, it is very important to label all the donor cells. Freshly harvested BM-MNCs from Balb/c nu/nu mice were labeled with 0.4 mg/mL Cy5.5 and 0.1 mg/mL AF750, which did not show obvious cytotoxicity or growth inhibition (Supplemental Figs. S2 and S3). Furthermore, the NIRF dyes did not affect the colony-forming efficiency at these concentrations (Fig. 1A). BM-MNCs were efficiently labeled regardless of cell size and diversity (Fig. 1B). Using the NIRF dyes, homogeneous labeling on the cell surfaces was achieved despite using a variety of cell populations (Fig. 1C).

Fluorescence on the cell surface is retained and does not influence surface antigen recognition

Balb/c Sp-MNCs were double-stained with CFSE and NIRF dyes, and their mean fluorescence intensity (MFI) was measured every 24 h until 72 h using FACS (Fig. 1D). To activate and expand Sp-MNCs, we cultured them with CD3/28 beads and mIL-2. MFI of CFSE decreased by 1 log during the first 24 h, while MFI of NIRF hardly changed for 24 h; it was halved following cell division after 48 h. Because Sp-MNCs were labeled using the same method, the difference in MFI between CFSE and NIRF can be attributed to the faster fluorescence decay of CFSE, as its excitation wavelength is in the visible range, rather than a difference in dye retention time on the cell surface. These results indicate that NIRF retains more stable MFI than CFSE.

During in vivo fluorescence imaging, recipient mice received approximately 20 excitations over a 24-h period. We confirmed that repeated excitations did not influence cell viability (Supplemental Fig. S4) or the NIRF MFI on the cell surface (Supplemental Fig. S5). It was also considered that precise evaluation of the obtained fluorescence images would be influenced by transfer of the NIRF dye from the donor cells to neighboring recipient cells after BMT and that the NIRF dyes on the cell surface would hinder recognition of cell surface markers. To examine these possibilities, we co-cultured Balb/c-derived $Thy1.2^+$ Sp-MNCs (NIRF labeled) and FVB/N-derived $Thy1.1^+$ cells for 3 h and examined their NIRF-labeling status and recognition by corresponding antibodies using FACS. The cells labeled with NIRF were recognized as $Thy1.2^+$. Co-cultured $Thy1.1^+$ cells showed no increase in NIRF (Fig. 1E). These results indicate that NIRF dyes were universally retained on the cell surface and did not influence the recognition of cell surface antigens, suggesting that in vivo fluorescence imaging with NIRF-labeled cells would contribute to acquisition of spatiotemporal information regarding donor cells shortly after BMT.

In vivo tracking of Cy5.5-labeled hematopoietic cells during the first 24 h after BMT

Cy5.5-labeled Balb/c nu/nu BM-MNCs were transplanted to the Balb/c nu/nu recipient mice. Since abdominal autofluorescence caused by food decreases the precision of in vivo imaging, all mice were fasted before in vivo imaging to suppress autofluorescence from food particles in the GI tract, (Supplemental Figs. S1 and S6). The Cy5.5 signal was observed from both sides of the tibiae and spines at 5 min after BMT through the tail vein (Supplemental Fig. S7). We further examined the status of transplanted BM-MNCs with Cy5.5 labeling (Fig. 2) and found that BM-MNCs from ICR/EGFP were homogeneously labeled with Cy5.5 on the cell surface (Fig. 2A). FACS analysis revealed that the $EGFP^+$ cells included all leukocyte fractions (Fig. 2B).

To confirm whether the in vivo Cy5.5 signals from the tibia (Supplemental Fig. S7) were derived from Cy5.5-labeled transplanted BM-MNCs, we transplanted Cy5.5-labeled ICR/EGFP BM-MNCs to the Balb/c nu/nu mice. Cy5.5 signals were observed in the tibia 24 h after BMT; these signals decreased thereafter (Fig. 2C). BM cells in the tibia were flushed and then observed by fluorescence microscopy on the same schedule as for in vivo imaging. We confirmed that the Cy5.5 signals detected in the tibia 24 h after BMT were from the transplanted BM-MNCs and belonged to the $Cy5.5^+$ and $EGFP^+$ cell populations (Fig. 2C, upper row). The cell surface Cy5.5 signal decreased throughout the experiment, probably due to cell division (Fig. 2C), while the chimerism of the $EGFP^+$ cells increased rapidly (Fig. 2D). The NIRF signals emanating from the transplanted donor cells decreased with inverse proportion to cell division.

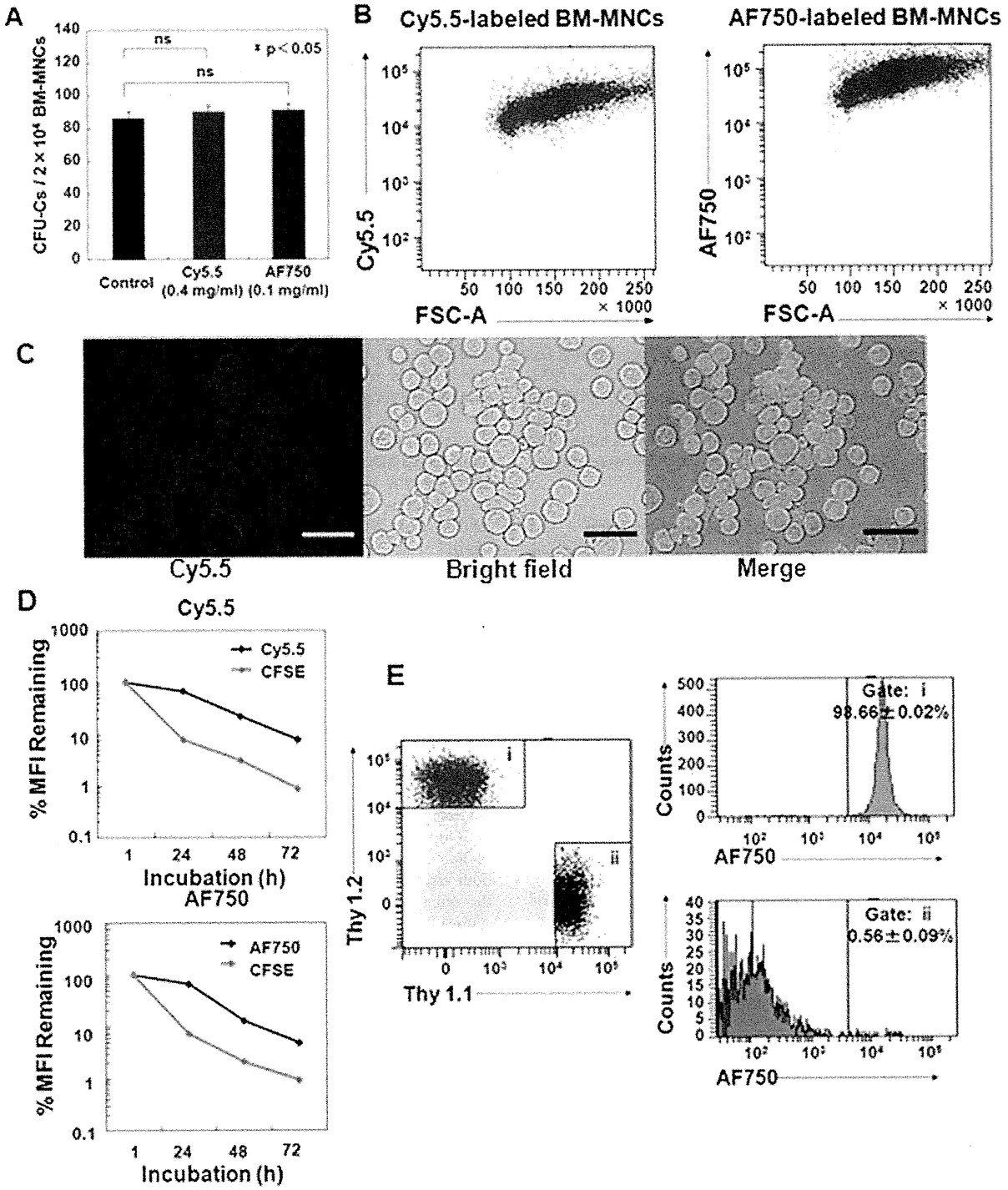

Figure 1. Evaluation of cytotoxicity and in vitro fluorescence intensity of NIRF labeling. (A) GM-CFUs, BFU-Es, and CFU-GEMMs were counted (n = 5); mean CFUs per 2×10^4 BM-MNCs are shown. (B) FACS analysis of Balb/c nu/nu BM-MNCs labeled with Cy5.5 (0.4 mg/mL) and AF750 (0.1 mg/mL). (C) Representative fluorescence image of Cy5.5-labeled Balb/c nu/nu BM-MNCs. Bar = 100 μm. (D) In vitro retention of NIRF and CFSE in Balb/c Sp-MNCs for the indicated times after labeling (n = 8). Sp-MNCs (1×10^5) were seeded in a 96-well plate with phenol red-free RPMI 1640 medium containing CD3/28 beads and mIL2. Values are %MFI ± SEM. Error bars are less than 1.1%. (E) AF750-labeled Balb/c Thy1.2$^+$ Sp-MNCs (1×10^6) (i) were mixed in a 1:1 ratio with unlabeled FVB/N Thy1.1$^+$ Sp-MNCs (1×10^6) (ii) at 37°C for 3 h, and the AF750 intensity of Thy1.1$^+$ and Thy1.2$^+$ cells was analyzed by FACS.

doi:10.1371/journal.pone.0011114.g001

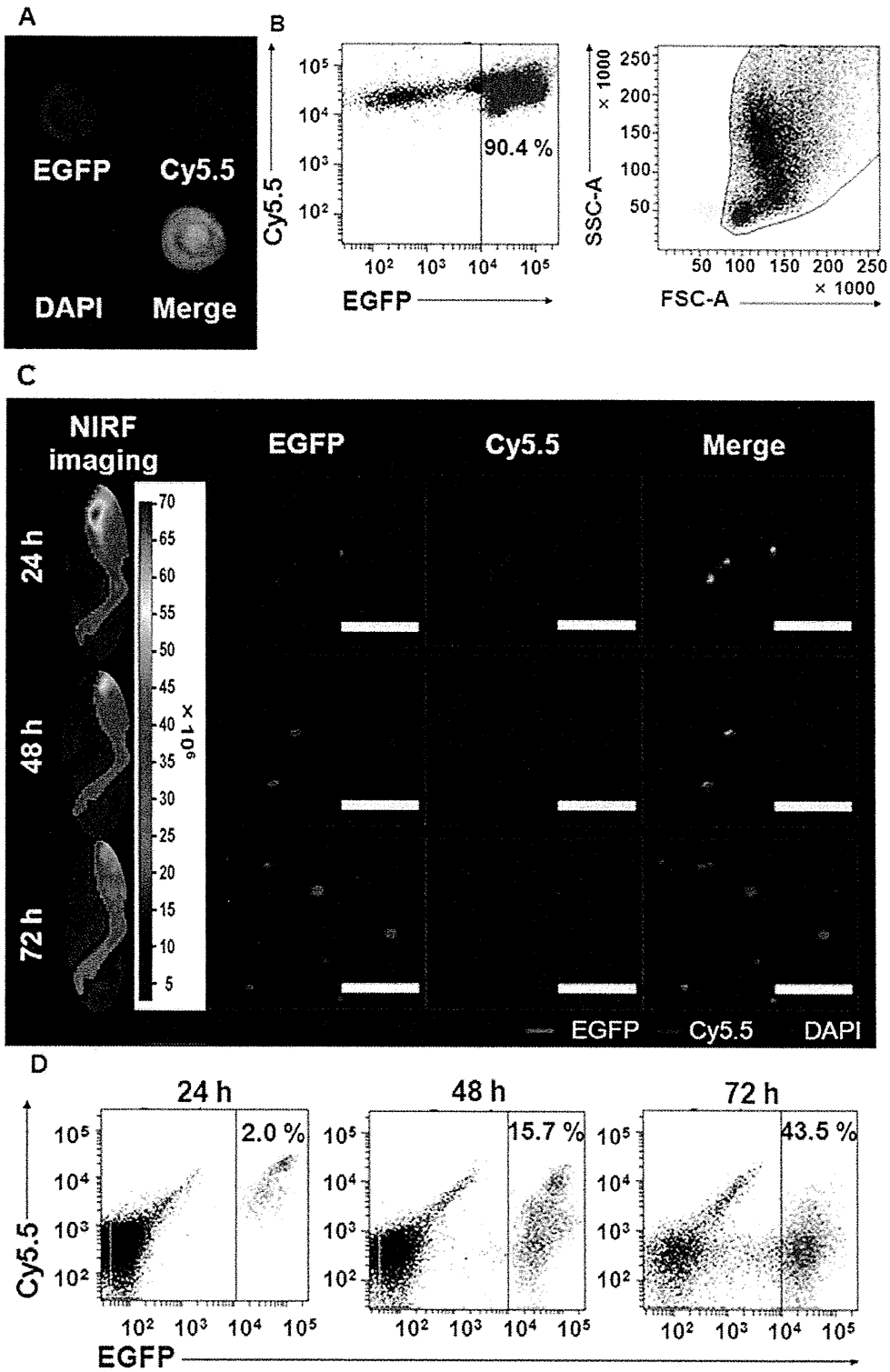

Figure 2. EGFP and Cy5.5 double-positive cells were detected in BM at 24 h after BMT. (A) Representative fluorescence image of Cy5.5-labeled ICR/EGFP BM-MNCs. Green, EGFP; blue, DAPI; red, Cy5.5. (B) FACS analysis of Cy5.5-labeled ICR/EGFP BM-MNCs at 1 h after labeling. The $EGFP^+$ cells included all leukocyte fractions. (C) Analysis of Cy5.5 and EGFP double-positive cells in the tibiae at the indicated times. Recipient Balb/c nu/nu mice ($H\text{-}2^d$) were transplanted with 1×10^7 Cy5.5-labeled ICR/EGFP BM-MNCs (closed colony). In vivo fluorescence imaging of the right legs of mice

transplanted with Cy5.5-labeled BM-MNCs obtained from ICR/EGFP mice is shown (left column). The cells from the tibiae were observed under an inverted fluorescent microscope (right column). Bar = 40 μm. Green, EGFP; blue, DAPI; red, Cy5.5. (D) FACS analysis of chimerism of Cy5.5 and EGFP double-positive cells in the tibiae at the indicated times.
doi:10.1371/journal.pone.0011114.g002

Evaluation of in vivo imaging of NIFR-labeled donor cells revealed that the NIRF tracking approach is highly sensitive

Next, we transplanted AF750-labeled ICR/EGFP BM-MNCs into the Balb/c nu/nu mice to evaluate the sensitivity and accuracy of our approach for tracking the homing process of donor cells in vivo. Distribution of the donor cells was monitored using an in vivo imaging device for 24 h after BMT. Using AF750-labeled cells, transplanted cells were detected in many organs in vivo (Fig. 3A). The distribution of donor cells was spread over several organs including the lung, liver, spleen, and BM (Fig. 3B). Ex vivo imaging of the recipient mice at 24 h after BMT confirmed NIRF signal distribution in the tissues suggested by in vivo imaging (Fig. 3C). Significant NIRF signals were detected in BM and the reticuloendothelial system, but not in the GI tract (Fig. 3C). To confirm the presence of donor cells in the tissues detected by ex vivo fluorescent imaging, sections of the tissues were examined for presence of $EGFP^+$ cells 24 h after transplantation (Fig. 3D). Although significant fluorescent signals were detected in the tissues by in vivo and ex vivo imaging, the $EGFP^+$ cells were sparsely distributed in each tissue, indicating that in vivo NIRF imaging is highly sensitive.

In vivo and ex vivo tracking of AF750-labeled cells in various congenic BMT models in an initial phase after transplantation

The above results strongly suggest that in vivo imaging of NIRF-labeled donor cells would provide a highly sensitive and accurate method to track the homing process of transplanted cells. First, congenic BMT was performed to evaluate the homing process of transplanted cells in the absence of rejection. Biodistributions of the transplanted BM-MNCs labeled with AF750 were then compared in various congenic BMT models at an early stage after transplantation. The AF750 images obtained after injection of NIRF-unlabeled BM-MNCs were identical to those of the background signals in PBS-injected mice (Supplemental Fig. S8). After intravenous injection of free AF750, the fluorescent signal disappeared through the urinary system within 1 h after BMT (Supplemental Fig. S8). In the congenic BMT model mice, the fluorescent signal was detectable in both tibiae 5 min after transplantation. It gradually increased by 3 h and remained unchanged for the rest of the observation period (Fig. 4A, supine position). We detected transplanted cell homing in vivo at 5 min after BMT, which is the earliest detection time reported thus far. In the reticuloendothelial system, the transplanted cells were first seen trapped in the lung 5 min after BMT and then in the liver and spleen 15 min after BMT. In the IBM-BMT model, the transplanted cells were seen trapped in the lung through the peripheral circulation 5 min after IBM-BMT (Fig. 4A, supine position). In this model, the donor cells migrated from the left tibia to the right one within 1 h after BMT (Fig. 4A, supine position), although many cells stayed in the left tibia for 24 h. Tissue distribution of the fluorescent signal was examined by ex vivo imaging 24 h after BMT in both BMT models. When the free AF750 dye was injected intravenously, the background level slightly increased in each organ, although the increase was negligible (Fig. 4B). In a comparison of congenic BMT with congenic IBM-BMT (Fig. 4B), most of the donor cells were found to remain in the injected left tibia in congenic IBM-BMT mice, while most of the donor cells migrated to all bones of the body in the congenic BMT mice. To our knowledge, this is the first report using in vivo imaging to reveal the distribution dynamics of transplanted cells after IBM-BMT, and the results suggest that the NIRF labeling approach would be applicable in various congenic BMT models.

Transplanted donor cell division starts more than 24 h after BMT

To determine the start time of transplanted donor cell division after homing, we harvested the cells from the tibiae and peripheral blood of the recipient mice at 24, 48, and 72 h after transplantation of AF750-labeled ICR/EGFP BM-MNCs and examined the fraction of $EGFP^+$ cells present by FACS (Fig. 5A). The NIRF intensity of $EGFP^+$ cells 24 h after BMT was similar to that of preBMT cells (Figs. 5A, B second row), indicating that the donor cells had not started cell division until then because NIRF intensity decreased with cell division (Fig. 1D, Supplemental Fig. S3). Donor cell division started thereafter because the chimerism of $EGFP^+$ cells in the tibiae of the recipients increased by approximately 45% at 72 h after BMT (Figs. 5B, C). FACS analysis revealed that the donor cell population contained all leukocyte fractions at 72 h after BMT (Fig. 5B, top right panel) and that $EGFP^+$ appeared in the peripheral blood at 72 h with similar fluorescence intensity as that in BM (Fig. 5D, Supplemental Fig. S9).

Immunohistochemical analysis confirmed that the number of transplanted $EGFP^+$ cells did not increase until 24 h after BMT and then rapidly expanded in the epiphyseal area of the tibia and femur between 48 and 72 h after BMT (Figs. 5E, F). These results indicate that transplanted donor cell division starts more than 24 h after BMT and that hematopoietic reconstitution in Balb/c nu/nu recipient mice begins approximately 72 h after BMT.

In vivo and ex vivo tracking of AF750-labeled cells in various allogeneic BMT models

We attempted to visualize the biodistribution of allogeneic BMT models with C57BL/6 (as donors) and Balb/c nu/nu mice (as recipients) to analyze the onset of aGVHD. Because the depletion of donor T cells abrogates GVHD [15], TCD-BMT (nonGVHD) and TCD-BMT plus Sp-MNCs (GVHD) transplantation models were established. In allogeneic BMT and the GVHD models, the fluorescent signals from the reticuloendothelial system were very high at 24 h after BMT (Fig. 6A, right top and bottom panels). The tissues with a high fluorescent signal were confirmed by ex vivo imaging 24 h after BMT (Fig. 6B). Among the reticuloendothelial system, the fluorescence was lowest in the nonGVHD model and highest in the GVHD model (Fig. 6B). These results indicate that the presence of a T-cell population in the donor cells causes homing to the reticuloendothelial system and that the TCD donor cells predominantly homed to BM. The fluorescent signal was very weak in the intestinal tract in all allogeneic BMT models (Fig. 6B, bottom row).

Discussion

To our knowledge, this study is the first report describing the use of in vivo real-time imaging to visualize the distribution dynamics of transplanted BM cells in the entire body during the

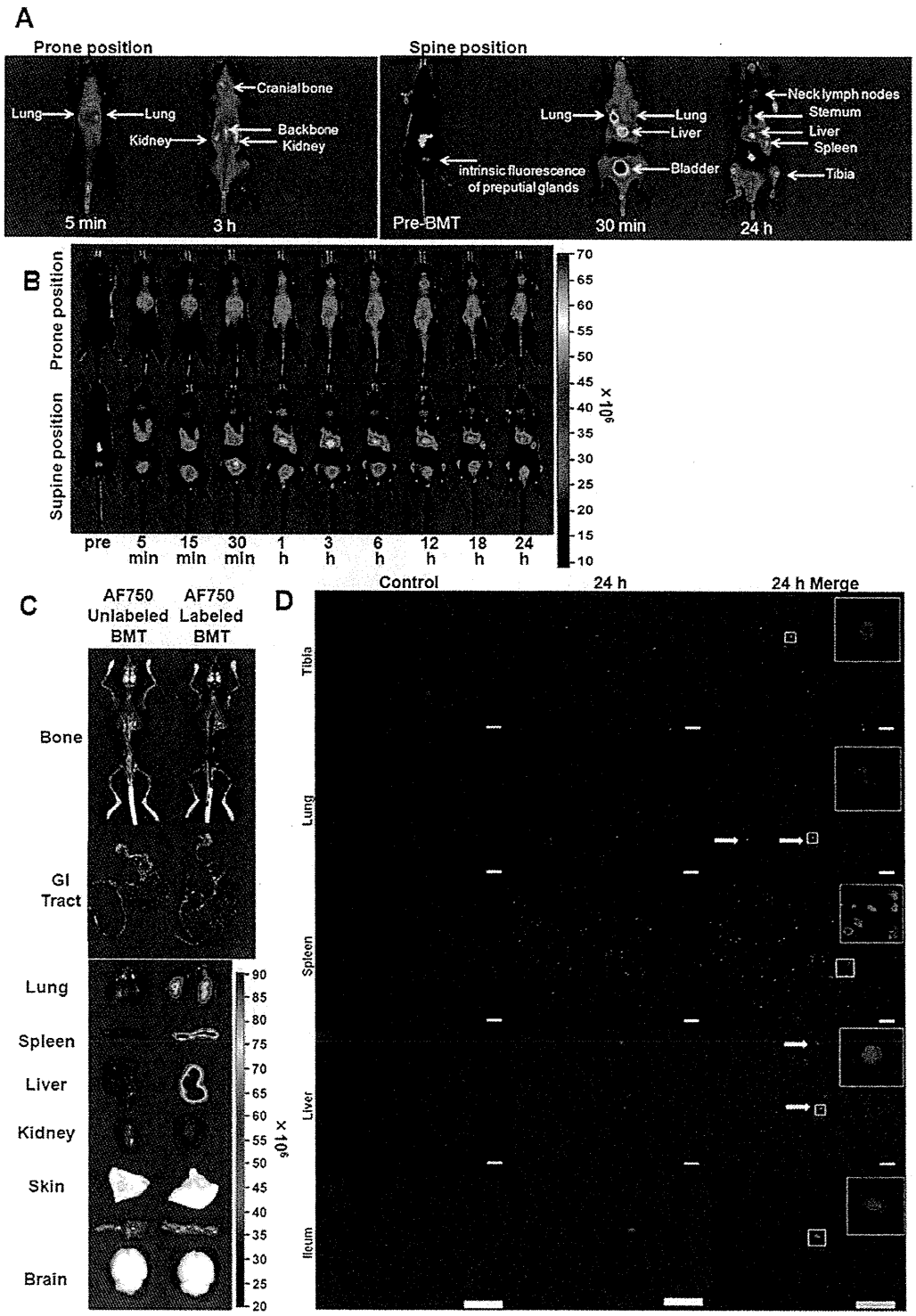

Figure 3. Fluorescent signals from AF750/EGFP double-positive cells were detected in vivo with extremely high sensitivity. Lethally irradiated Balb/c nu/nu (H-2^{d}) mice were transplanted with 1×10^{7} AF750-labeled ICR/EGFP BM-MNCs. (A) Sources of NIRF signals in vivo. The congenic BMT model is shown as an example. (B) Representative in vivo images of the recipient mice at the indicated times after BMT. The prone (upper row) and supine (bottom row) positions are shown. (C) Ex vivo imaging of the recipient mice. Mice transplanted with AF750-labeled (left) or unlabeled (right) BM-MNCs were sacrificed at 24 h after BMT. The congenic AF750-unlabeled BMT model is shown as a control. (D) Fluorescence images of various organs from recipient mice. AF750-labeled ICR/EGFP BM-MNCs were transplanted, and the organs were examined 24 h after

BMT. Untreated Balb/c nu/nu mice were used as controls. Green, EGFP; blue, DAPI. White arrows show EGFP/DAPI double-positive cells. Bar = 100 μm.
doi:10.1371/journal.pone.0011114.g003

initial phase after BMT using the NIRF method. Achieving in vivo imaging at a very early stage after BMT was previously difficult because the small number of cells that escape the reticuloendothelial system result in minute cell distributions within each organ. In this study, we labeled the surface of transplanted cells with NIRF and successfully demonstrated the altered distribution dynamics of transplanted cells in the initial phase. We could noninvasively track transplanted cells circulating in the entire body during the initial stage after BMT because of the following reasons: (1) NIRF illumination with higher light propagation and lower attenuation through the tissue was used as both excitation and emission light for imaging [16]; (2) homogeneous labeling on the cell surface with NIRF dyes was achieved despite a variety of cell populations; (3) NIRF-labeled transplanted donor cells had a constant MFI, detectable in vivo over a 24-h period; (4) Balb/c nu/nu mice (hairless mice) were used to enhance NIRF signal

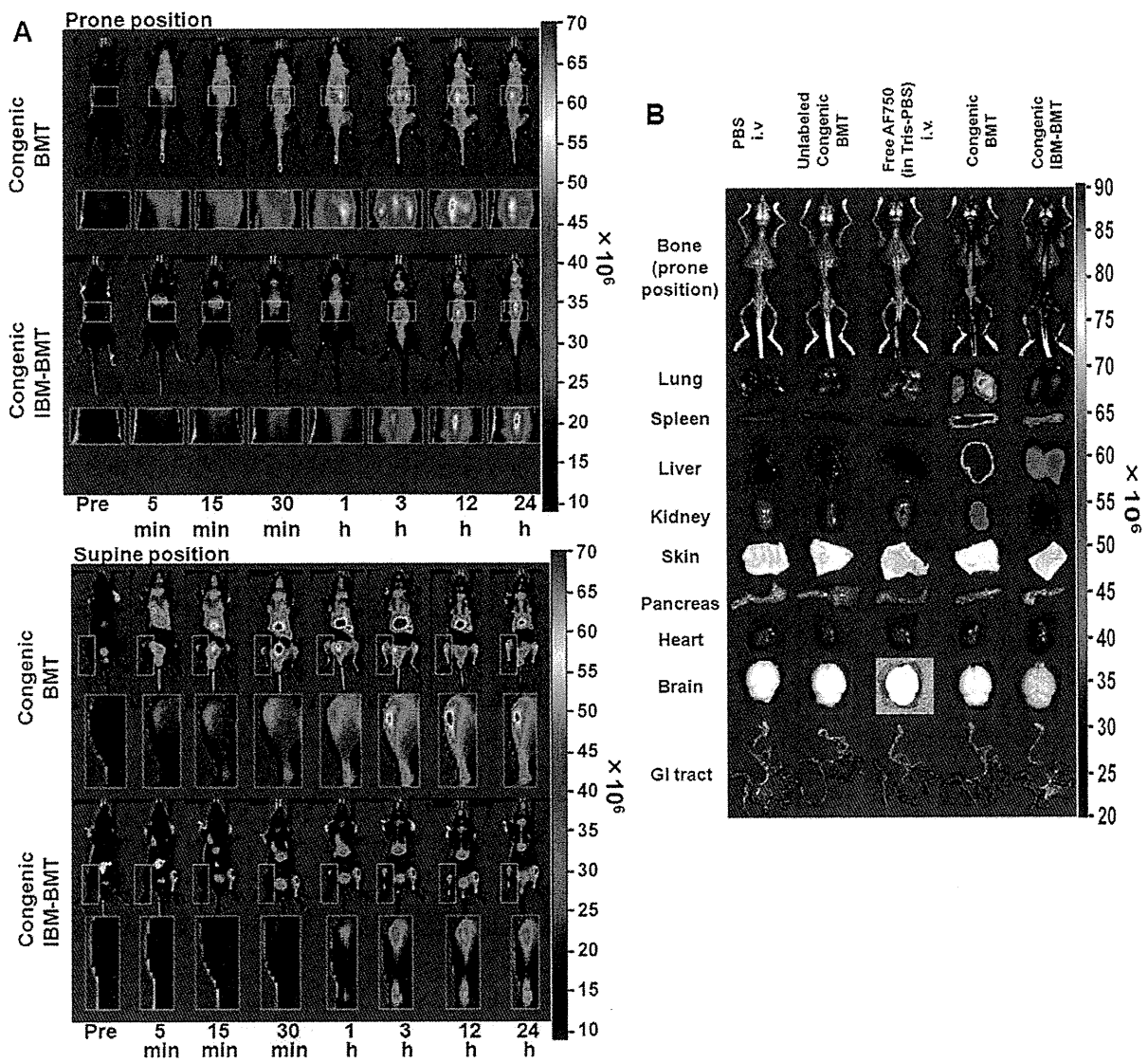

Figure 4. In vivo imaging of transplanted AF750-labeled donor cells in various congenic BMT models. (A) In vivo imaging of congenic BMT models until 24 h after BMT. In the congenic BMT model, the transplanted cells were detected in the tibiae at 5 min after congenic BMT (supine position). In the congenic IBM-BMT model, the migrating cells from the left tibia were detected 1 h after congenic IBM-BMT. The parts of the body with significantly increased signals (indicated by squares) were magnified and are shown below the corresponding whole-body images. (B) Ex vivo imaging of transplanted AF750-labeled donor cells in the BMT models at 24 h after BMT.
doi:10.1371/journal.pone.0011114.g004